

THESIS FOR THE DEGREE OF LICENTIATE OF ENGINEERING

Optical Guiding and Feedback in  
Gallium Nitride-Based Vertical-Cavity  
Surface-Emitting Lasers

Seyed Ehsan Hashemi



Photonics Laboratory  
Department of Microtechnology and Nanoscience (MC2)  
CHALMERS UNIVERSITY OF TECHNOLOGY  
Göteborg, Sweden, 2015

# Optical Guiding and Feedback in Gallium Nitride-Based Vertical-Cavity Surface-Emitting Lasers

Seyed Ehsan Hashemi

Göteborg, January 2015

©Seyed Ehsan Hashemi, 2015

Technical Report MC2-295  
ISSN 1652-0769

Photonics Laboratory  
Department of Microtechnology and Nanoscience (MC2)  
Chalmers University of Technology  
SE-412 96 Göteborg, Sweden  
Phone: +46 (0) 31 772 1000

Printed by Chalmers reproservice, Chalmers University of Technology  
Göteborg, Sweden, January, 2015

# Optical Guiding and Feedback in Gallium Nitride-Based Vertical-Cavity Surface-Emitting Lasers

Seyed Ehsan Hashemi  
Photonics Laboratory  
Department of Microtechnology and Nanoscience (MC2)  
Chalmers University of Technology  
SE-412 96 Göteborg, Sweden

## Abstract

The gallium-nitride (GaN) semiconductor material has been the core of the revolutionary breakthroughs during the last two decades in the lighting industry, by enabling manufacturing of efficient blue light emitting diodes (LEDs), for which the 2014 Nobel prize in physics was awarded. The GaN technology has further led to violet edge-emitting lasers (EELs), enabling the Blu-ray disk technology, and also to the commercialization of directly green emitting EELs. A natural next step is the realization of GaN-based vertical-cavity surface-emitting lasers (VCSELs), which has proved to be a challenging task. The first electrically injected GaN-based VCSEL was announced in 2008, more than a decade after the first reports on its EEL counterpart. Still today only four groups in the world have demonstrated lasing under continuous-wave operation in a blue VCSEL. Some of the major challenges to realize GaN-based VCSELs are the lack of two lattice matched materials for forming high reflectivity distributed Bragg reflectors (DBRs), the poor current spreading capabilities in p-doped GaN, and the difficulty to achieve current and optical confinement. In this work we have addressed those issues. We have developed the novel concept of  $\text{TiO}_2$ /air high contrast gratings (HCGs) to achieve high reflectivity over a broad wavelength range. The HCGs show a high reflectivity ( $>95\%$ ) over a 25 nm wavelength span, and a very good agreement between simulated and measured reflectivity spectra has been achieved. By using our in-house developed VCSEL simulation tools we have studied existing GaN-based VCSEL designs and shown that the approach taken by most groups to confine the current to the center of the device (transverse direction), yields an optical resonator that is weakly antiguiding with very high optical losses and thereby high threshold currents. These anti-guided devices have total losses that are typically 100-200% higher than in our newly proposed structures, in which current confinement and optically guiding can be achieved simultaneously. These structures have already been implemented by two of the world's leading groups in the area.

Keywords: vertical-cavity surface-emitting laser, gallium nitride laser, antiguiding,  $\text{TiO}_2$  high contrast grating



---

## List of Papers

---

This thesis is based on the following appended papers:

- [A] E. Hashemi, J. Gustavsson, J. Bengtsson, M. Stattin, G. Cosendey, N. Grandjean, and Å. Haglund, "Engineering the Lateral Optical Guiding in Gallium Nitride-Based Vertical-Cavity Surface-Emitting Laser Cavities to Reach the Lowest Threshold Gain," *Jpn. J. Appl. Phys.*, vol. 52, no. 8S, pp. 08JG04, May 2013.
- [B] E. Hashemi, J. Bengtsson, J. Gustavsson, M. Stattin, G. Cosendey, N. Grandjean, and Å. Haglund, "Analysis of structurally sensitive loss in GaN-based VCSEL cavities and its effect on modal discrimination," *Opt. Express*, vol. 22, no. 1, pp. 411–426, Jan. 2014.
- [C] E. Hashemi, J. Bengtsson, J. Gustavsson, M. Stattin, M. Glauser, G. Cosendey, N. Grandjean, M. Calciati, M. Goano, and Å. Haglund, "Triggering of guiding and antiguiding effects in GaN-based VCSELs," *Proc. SPIE, Vertical-Cavity Surface-Emitting Lasers XVIII*, vol. 9001, 90010A, Feb. 2014.
- [D] E. Hashemi, J. Bengtsson, J. Gustavsson, S. Carlsson, G. Rossbach and Å. Haglund, "TiO<sub>2</sub> membrane high-contrast grating reflectors for GaN-based vertical-cavity light emitters," *Submitted to Applied Physics Letters*.



---

## Acknowledgement

---

There are many who have supported me and contributed to an amazing experience of the PhD studies for me so far. I have had the privilege to work closely with three extremely talented people in this project. First of all, I am very grateful to my main supervisor Assoc. Prof. Åsa Haglund for accepting me as her first PhD student and never giving up on supporting me. Her cheerfulness, excitement, and engagement in the field has always motivated me to learn more and work harder. I am also very thankful to my co-supervisors Assoc. Profs. Jörgen Bengtsson and Johan Gustavsson. Thank you Jörgen for your help and supervision with all the simulation work, in-depth fruitful discussions, lifesaving comments and feedbacks, and pleasant lunch times. Thank you Johan for instructing me with the simulations and always coming up with brilliant ideas. I am also very grateful to Prof. Anders Larsson, my examiner, for the encouragements and guidance with my research work and the PhD studies. I am thrilled to have worked and will still be working in an exciting and delightful environment that my fellow colleagues have been a main part of it. A great deal of appreciation goes to Martin Stattin, Rashid Safaisini, and Erik Haglund, particularly for mentoring me in the cleanroom. I am also grateful to the very committed staff of MC2 Nanofabrication Laboratory for their technical support. I am happy to have shared nice memories with all of you opto dudes and fiber guys, thanks for being part of it. I also appreciate the contribution of our collaborators at EPFL in Switzerland and Politecnico di Torino in Italy in our joint publications.

I feel to be extremely lucky to have constantly received so much care and love from many individuals from near or far, my parents Parvin and Mohammad, and my brothers Pouyan and Kian in Iran, and in Sweden Parand, Payam, Faramarz, Damon, and Babak. Last but not least, I have no words to properly thank you my lovely Pardis, for all your passion, love, and encouragements.

Financial support from the Swedish Research Council (Vetenskapsrådet) and the Hasselblad Foundation are acknowledged.

Seyed Ehsan Hashemi

*Göteborg  
January 2015*



---

# Table of Contents

---

<b>Abstract</b>	<b>i</b>
<b>List of Papers</b>	<b>iii</b>
<b>Acknowledgement</b>	<b>v</b>
<b>1 Introduction</b>	<b>1</b>
1.1 Applications . . . . .	2
1.2 Thesis outline . . . . .	2
<b>2 III-N material properties</b>	<b>5</b>
2.1 Crystal structure and features . . . . .	5
2.2 The origin of polarization fields . . . . .	6
2.3 Optical properties . . . . .	6
2.4 Electrical properties . . . . .	7
<b>3 III-N VCSELs</b>	<b>11</b>
3.1 Major Challenges in GaN-VCSEL realization . . . . .	12
3.2 State-of-the-art technologies in GaN-VCSELs . . . . .	13
3.2.1 Hybrid DBR design . . . . .	13
3.2.2 Double dielectric DBR design . . . . .	14
3.2.3 Intracavity contact schemes . . . . .	16
3.3 Additional challenges to be addressed . . . . .	16
<b>4 Guiding/Antiguinding effects in GaN-based VCSELs</b>	<b>21</b>
4.1 Optical guiding study . . . . .	22
4.1.1 Hot-cavity: The effect of self heating . . . . .	23
4.2 The main conclusions . . . . .	26
<b>5 High contrast grating reflectors for GaN-based VCSELs</b>	<b>29</b>
5.1 Structural description . . . . .	29
5.2 Application of HCGs in VCSELs . . . . .	30
5.3 Fabrication of TiO <sub>2</sub> /air HCG . . . . .	31

5.3.1	Dielectric stack deposition . . . . .	32
5.3.2	Annealing . . . . .	32
5.3.3	Pattern definition and Ni lift-off . . . . .	33
5.3.4	Dry etching . . . . .	33
5.3.5	Wet etch sacrificial removal . . . . .	34
5.4	Characterization of TiO <sub>2</sub> /air HCG . . . . .	34
<b>6</b>	<b>Future outlook</b>	<b>37</b>
<b>7</b>	<b>Summary of Papers</b>	<b>39</b>
	<b>References</b>	<b>41</b>
	<b>Papers A–D</b>	<b>49</b>

# Chapter 1

---

## Introduction

---

The vertical-cavity surface-emitting laser, or VCSEL, is a major type of a semiconductor laser, the other major type being the edge emitting laser. In VCSELs the beam emission is perpendicular to the plane of the epitaxial layers in contrast to the edge emitting lasers which emit through the cleaved facets on the sides. Vertical surface emission has many advantages although it poses a lot more challenge on the production process. Favorable characteristics of VCSELs include a circular output beam profile, low threshold current, single longitudinal mode emission [1], higher modulation speed at low currents [2], two-dimensional (2D) array capability [3], and straightforward wafer-level device testing in production.

The history of VCSELs began in 1977, when Kenichi Iga established the concept and practically realized this new type of semiconductor laser [4, 5], which has over the years become the backbone light source of our data networks. The standard VCSELs emitting at infrared 850 and 980 nm wavelengths are now fully mature devices, and every year millions of them are produced, thanks to the progress that has been made in the gallium-arsenide (GaAs) material technology. The GaAs material properties are well-suited to monolithically grow the entire multilayer structure of a VCSEL with high optical, electrical, and thermal performance.

The success of GaAs-based VCSELs has tempted both researchers and industries to expand the emissions ranges towards shorter and longer wavelengths, where the properties of the suited materials are not equally favorable. VCSELs emitting in the visible regime are of high interest for many applications but will require a completely different class of materials with wide bandgaps in which the high quality (low defect) growth of multilayer structures are much more challenging at least with today's technologies.

To produce the blue and green emission in semiconductor lasers, materials with large *direct* bandgap are used. The three main types of such semiconductor materials are the group III-nitrides such as gallium-nitride (GaN), the group II-oxides such as

zinc-oxide (ZnO), and the group II-chalcogenides such as zinc-selenide (ZnSe) [6]. In the race between these three types of semiconductor compounds, GaN has become dominant in the last 20 years thanks to the revolutionary work done in late 80's and early 90's to make GaN-based p-n junctions, which facilitated the production of high power light emitting devices [7, 8]. This progress in III-nitride materials has redirected the efforts that were previously devoted to the II-VI material system, in which for instance an electrically injected CdZnSe/ZnSe VCSEL emitting at 484 nm was demonstrated at 77 K [9]. The main difficulties with the II-chalcogenides and II-oxides are degradation under current injection and the p-doping, respectively.

### 1.1 Applications

As mentioned, to move towards the visible regime will enable new applications in which there is a need for compact, efficient, and low cost light emitters [10–13]. In some of the applications such as printers and high-density data storage, a shorter wavelength means a higher available resolution or capacity. Besides, RGB (red-green-blue) VCSELs may be used in heads-up displays and micro-projectors. Microcavity lasers in particular can easily be integrated into portable equipment and lab-on-chip.

Applications in the fields of biology and biomedicine, e.g. biosensors, may also benefit from having laser light with high beam quality in the range of 400–500 nm wavelength. Some of the examples include chemical tracking and biological agent detection based on exciting a dye molecule fluorescein around 494 nm and study the fluorescence. In optogenetics, stem cells can be genetically modified to render them sensitive to blue light; thereby, events in specific cells of living tissue can be controlled, with applications in artificial ears or eyes. Blue resonant light-emitters could enable novel designs and facilitate system integration into the body. In medical diagnosis, skin and esophagus cancer detection have become possible, without the use of biopsy, by using laser-induced fluorescence at a wavelength of 410 nm [14, 15]. This non-invasive technique is fast, reliable and reduces both pain and recovery time for the patient.

Recently, it has been noted that industries are counting on semiconductor lasers to make the future of the solid state lighting applications due to their higher efficiencies at high drive current densities [16, 17]. Shuji Nakamura, who received the physics Nobel prize in 2014 for his work on efficient blue light emitting diodes (LEDs) mentioned at the Nobel prize ceremony that "Laser lighting could replace all of conventional LED lighting in the future, in order to reduce costs, in order to increase efficiency further," [18].

These are only a few of the many applications for UV-blue-green microcavity lasers and RCLEDs that can be foreseen, and many more will appear once such light sources actually exist.

### 1.2 Thesis outline

In this thesis, VCSELs based on the GaN material system have been explored, which are intended to emit at violet-blue (420–450 nm) wavelengths. Consequently, in

the next chapter some of the important material properties of the group III-nitride semiconductors are addressed. In chapter three, the state of the art electrically injected GaN-based VCSELs that have been realized so far are discussed in order to make a comparison between the competing technologies. Moreover, some of the fundamental challenges related to the remaining device shortcomings are introduced. In chapter four, our work on how current aperture schemes can dramatically change the optical guiding, and thus the threshold current, is presented. In chapter five, a new method to fabricate the top reflector of nitride VCSELs based on a titanium-dioxide ( $\text{TiO}_2$ )/air high contrast grating is demonstrated. At the end an outlook about the prospects of III-nitride based VCSELs is given.



# Chapter 2

---

## III-N material properties

---

### 2.1 Crystal structure and features

III-N semiconductors such as GaN, or more generally (Al, In, Ga)-N alloys, can be epitaxially grown to different atomic structures, so called polytypes [19]: either wurtzite or zincblende. The wurtzite structure is the one which is thermodynamically stable under ambient conditions and therefore there is an intrinsic tendency for formation of this polytype. The zincblende can be stabilized by epitaxial growth of thin films on specific crystal planes of cubic substrates such as Si [20], SiC [21], and GaAs [22]. The zincblende has a cubic unit cell with a crystal structure identical to that of diamond (two interpenetrating face-centered cubic sublattices with an offset of one-quarter of distance along a body diagonal).

On the other hand, wurtzite, the more important polytype of III-nitrides, has a hexagonal unit cell and thus two lattice constants,  $c$  and  $a$ . The crystal structure, which is shown in a stick and ball representation in Fig. 2.1, is formed by two interpenetrating hexagonal close-packed (hcp) sublattices, each with one type of atom, displaced with an offset of  $\frac{5}{8} \cdot c$  along the  $c$ -axis. Therefore it can be identified by alternating biatomic close-packed (0001) planes of Ga and N pairs [19].

Some of the basic features of the wurtzite crystal structure are:

- The lack of the inversion symmetry along (0001) surface, which leads to two types of polarity: Ga polar, and N polar [23].
- The  $u$  parameter, which is defined as the ratio between the length of the anion-cation bond and the  $c$  lattice parameter, is ideally  $\frac{3}{8} = 0.375$ .
- The three crystal planes of special importance: (0001) the  $c$ -plane, ( $1\bar{1}00$ ) the  $m$ -plane, and ( $11\bar{2}0$ ) the  $a$ -plane.

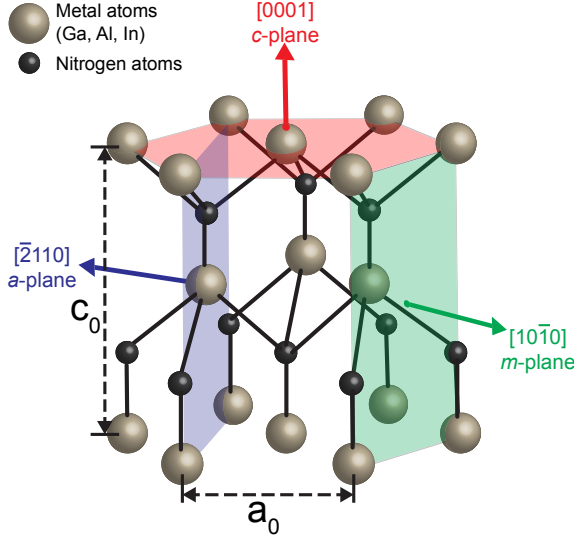


Figure 2.1: A stick and ball representation of the wurtzite crystal structure with Ga polarity (0001).

## 2.2 The origin of polarization fields

The wurtzite crystal is non-centrosymmetric, and due to the lack of inversion symmetry along (0001)-plane it is therefore polar along the c-axis. Due to this polarity strong polarization fields are present in the III-nitride semiconductors. Even in an ideal wurtzite structure a non-vanishing spontaneous polarization is present due to the difference in electronegativity (electron cloud being closer to the nitrogen atoms), see Fig. 2.2. In particular at a heterointerface between two nitride semiconductors, for example GaN and AlN (presumably with no strain), this spontaneous polarization gives rise to boundary effects due to the varying electronegativity of the nitrides.

Moreover if the crystal is strained along the (0001)-plane, due to the difference between the lattice parameters or the thermal expansion coefficients in the heterostructure, the piezoelectric effect can induce a polarization field. Therefore the piezoelectric polarization field is different depending on the type of the strain being tensile or compressive. The direction of the piezoelectric polarization field is presented in Fig. 2.2 for a Ga polarity with an in-plane compressive strain. The details of both types of polarization fields are discussed in refs. [19, 24].

## 2.3 Optical properties

The wurtzite polytypes of GaN, AlN, and InN form a continuous alloy system whose direct bandgaps range from 0.7 to 6 eV, corresponding to the wavelength emissions

from red to UV, see Fig. 2.3. The materials are uniaxially birefringent, again due to the polarity of the wurtzite crystal along the c-axis. Figure. 2.4 shows the dispersion of the anisotropic complex refractive index  $(n,k)$  for GaN and AlN [25]. These optical constants have been experimentally studied and the main causes of the mentioned anisotropy have been attributed to the special features of the band structures [26, 27].

The internal electric fields in the order of 10 MV/cm that arise from the polarization fields in polar materials are large enough to separate the electron and holes towards opposite sides of a quantum-well (QW) layer, as illustrated in Fig. 2.5. This effect known as the Quantum Confined Stark Effect (QCSE), leads to a reduction of photon emission rate as the overlap between the electron and hole wave functions are reduced and also to a red shift in the photoluminescence peak [28–30]. However at high pump current densities, typical for laser operation, these internal fields can be screened by the injected carriers [31].

## 2.4 Electrical properties

As-grown undoped GaN has typically a large unintentional background electron concentration of about  $10^{16} \text{ cm}^{-3}$ , which is attributed to the formation of nitrogen vacancies or unintentional incorporation of oxygen impurities in the lattice, acting like donors [32]. Intentional n-type doping is often done by incorporation of Si im-

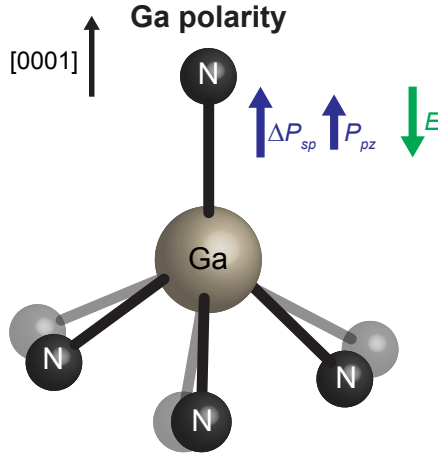


Figure 2.2: A tetrahedron with Ga polarity is shown in two different situations; without strain (light gray) and with compressive strain applied (darker gray) in the c-plane.

## 2. III-N MATERIAL PROPERTIES

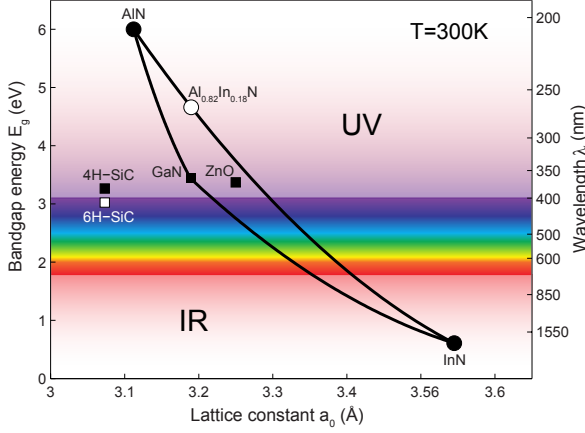


Figure 2.3: Room temperature bandgap of wurtzite III-nitride compounds versus the basal plane lattice constant  $a_0$ . By tuning the molar composition of the alloys it is possible to continuously tune the bandgap from ultraviolet (UV) to infrared (IR) energy. The square markers correspond to some of the important substrates. However, sapphire as the most often used substrate lies outside of the graph with a lattice constant  $a_0=4.765$  Å. It is also important to note the lattice matching between GaN and the AlInN alloy with 18% In content.

purities, which have a fairly low ionization energy of 20 meV [33], resulting in most donors being ionized at room temperature. Typical mobility values lie in the order of  $500 \text{ cm}^2\text{V}^{-1}\text{s}^{-1}$  at room temperature. On the other hand, p-type doping of GaN

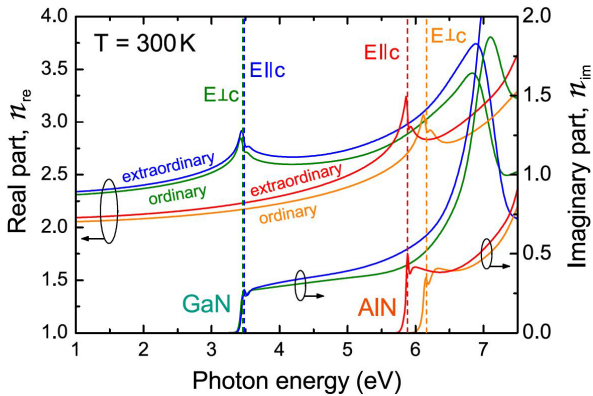


Figure 2.4: Anisotropic complex refractive index for GaN and AlN. Adapted from [25].

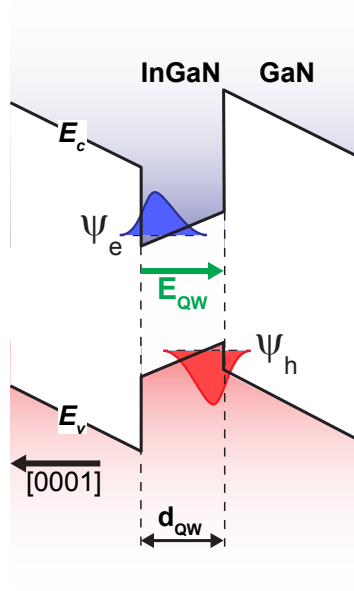


Figure 2.5: Quantum confined Stark effect in InGaN QWs

is reputedly very challenging. Mg impurities are often used as acceptors to dope the GaN but their rather high ionization energy of 170 meV [34] leads to only a partial ionization of typically a few percent. Moreover, the mentioned background doping has n-type characteristics that lowers the actual hole concentrations, hindering the creation of an effectively p-doped material. The difficulty to p-dope GaN is a major problem for the device realization.



# Chapter 3

---

## III-N VCSELs

---

The attractive properties of VCSELs that were discussed in Chapter 1 are the main driving forces for the development of these devices also in the GaN material system. Some applications that can be expected for such GaN-based VCSELs are mentioned in Chapter 1. Looking at the history of GaN-based light emitters, major breakthroughs came in 1989 when Hiroshi Amano et al. [7] showed p-type conductivity in Mg-doped GaN material, which led to the first demonstration of high power GaN LEDs in 1991 by Shuji Nakamura [8]. In 1996 Nakamura also demonstrated the first continuous-wave (CW) operation of a GaN-based edge emitting laser diode at room-temperature (RT) [35]. Already in 1999 Nichia Corp. started to commercialize their first prototypes of GaN based edge emitting laser diodes, and soon lasers emitting at 405 nm wavelength, with several hundred mW output power and tens of thousands of hours lifetime, were available from multiple commercial sources. The first Blu-ray systems in optical data storage were introduced in 2004 using InGaN laser diodes emitting at 405 nm [36].

The progress in nitride VCSELs has however been much slower, starting with a few sporadic reports of lasing under optical pumping [37, 38] in addition to a few simulation works proposing different structures for nitride VCSELs [39, 40]. In 2008, in separate works, researchers from National Chiao Tung University (NCTU) in Taiwan and Nichia Corp. in Japan finally showed the two first electrically injected CW operations of GaN-VCSELs at 77 K [41] and at RT [42], respectively. The long time span between the edge emitting laser and the VCSEL shows that the GaN technology was not mature and developed enough to meet the requirements of VCSEL production. Improvements in both output power and lifetime of today's nitride VCSELs are required before they can be of any real practical and commercial importance.

To develop better GaN-based VCSELs the shortcomings of the current devices both in terms of the material constraints and the technological limitations must be

understood. The focus should be at first to minimize the optical losses in the cavity in a step-by-step manner so that a high quality factor cavity and a low threshold condition can be achieved. The optical losses are believed to be caused by the low reflectivity of the DBRs, the absorption in the cavity, and the scattering losses due to inhomogeneities. One type of often overlooked loss related to GaN VCSELS will be presented later in this chapter. However not only the cold-cavity but also the hot-cavity properties have to be addressed. At higher injection currents, close to the actual operational current densities needed for lasing self-heating can increase the losses by changing the material properties with temperature. These effects have to be accounted for to be able to obtain a higher output power with a longer lifetime in these devices.

Therefore in this chapter we start by discussing the major challenges in GaN-based VCSELS, and then try to summarize and make a comparison between the cutting-edge technologies that have been employed so far by the different groups that have successfully achieved a lasing device under electrical injection. Moreover, based on these devices we can identify some extra constraints that might limit the performance of those devices.

### 3.1 Major Challenges in GaN-VCSEL realization

A GaN-based VCSEL with acceptable performance should most probably have the following features:

- High-reflectivity, broadband mirrors
- Uniform lateral current distribution
- Current and optical confinement with low optical loss

For the first item, the low refractive index contrast between GaN alloys necessitates a large number of DBR pairs in III-N based epitaxial DBRs, which results in a narrow reflectivity stopband. Moreover, the large lattice mismatch between these alloys makes it quite tricky to grow such large number of layers without cracks and dislocations. Ongoing research is being carried out by many groups to improve the growth of high quality nitride-based DBRs, but an alternative solution might be deposited dielectric DBRs for one or both of the mirrors needed in the VCSEL. In Section 3.2, we consider both approaches in the application of DBRs in VCSELS and discuss the advantages and the shortcomings of each solution.

The second item is important because the lateral current distribution in p-GaN material is relatively non-uniform since it is very difficult to obtain high-levels of p-type doping and thus high concentration of holes and high electrical conductivity in p-type GaN material. Therefore, current crowding prevents a uniform injection of carriers into the active region. Intracavity contacts employing a current spreading layer have been widely used to overcome this problem, although this is not quite straightforward. Section 3.2.3 deals with issues regarding intracavity contacts and current spreading layers.

The third item stresses the importance of ensuring confinement of both carriers and photons to the center of the device without increasing the optical losses in

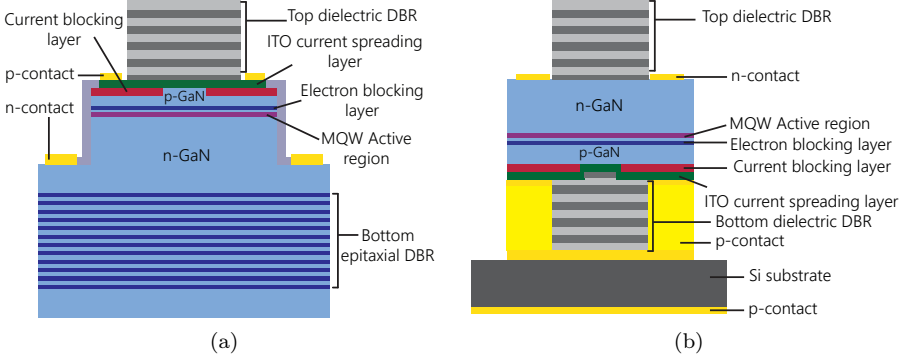


Figure 3.1: GaN VCSEL structure with a (a) hybrid DBR scheme (b) double dielectric DBR scheme.

the cavity. In Section 3.3, the limitations of the common methods of both current and photon confinements in GaN-based VCSELs are investigated and some further possible limitations for the performance of these devices are discussed.

## 3.2 State-of-the-art technologies in GaN-VCSELs

The research groups that have obtained functioning GaN-based VCSELs have used either a hybrid scheme for the DBR or an entirely dielectric solution, as illustrated in Fig. 3.1. In the hybrid scheme one of the DBRs is grown epitaxially and the other is made of deposited dielectric materials.

The available details of the VCSEL structures that were used by the different groups are listed in Table 3.1 and the obtained results for each of those devices are reviewed in Table 3.2. All structures are grown on c-plane if not stated otherwise.

### 3.2.1 Hybrid DBR design

Among the different research groups, only two have taken this approach, the National Chiao Tung University (NCTU) in Taiwan with an AlN/GaN DBR [50] and EPFL in Switzerland with an AlInN/GaN DBR for the bottom reflector [51]. The AlN/GaN option delivers slightly higher refractive index contrast but there is about 2.5 % difference in the in-plane lattice constant between the two alloys, see Table 3.3. Given the large number of required DBR pairs (about 30) and the large lattice mismatch the researchers at NCTU had to use some sophisticated tricks to lower the density of cracks. In order to reduce the tensile stress, a short-period superlattice (SPSL) of AlN/GaN was placed after every 5<sup>th</sup> DBR period for the first 20 pairs and after every 3<sup>rd</sup> DBR period for the last 9 pairs. In this way, they could achieve a top reflectivity of 99.4% with 25 nm bandwidth. Gatien Cosendey and coworkers at EPFL took a lattice-matched (LM) approach using a combination of Al<sub>0.82</sub>In<sub>0.18</sub>N

### 3. III-N VCSELS

Table 3.1: Comparison between the structural designs of GaN-based VCSELS

	NCTU 2008/2010 [41, 43]	Nichia 2008 [42]	Nichia 2009/2011 [44, 45]	Panasonic [46]	UCSB [47]	EPFL [48]	Xiamen [49]
Top DBR	(8×)/(10×) Ta <sub>2</sub> O <sub>5</sub> / SiO <sub>2</sub>	(7×) Nb <sub>2</sub> O <sub>5</sub> / SiO <sub>2</sub>		ZrO <sub>2</sub> / SiO <sub>2</sub>	(13×) Ta <sub>2</sub> O <sub>5</sub> / SiO <sub>2</sub>	(7×) TiO <sub>2</sub> / SiO <sub>2</sub>	(14×) ZrO <sub>2</sub> / SiO <sub>2</sub>
Current spreading layer	240 nm ITO /(30 nm ITO + 2 nm p <sup>+</sup> -InGaN)	50 nm ITO		100 nm ITO	50 nm ITO + 14 nm p <sup>++</sup> -GaN	50 nm ITO + 20 nm p <sup>+</sup> -GaN	30 nm ITO + 2 nm n-InGaN
p-GaN thickness	120 nm/ 110 nm				113 nm	97 nm	159 nm
Aperture	200 nm SiN <sub>x</sub>	SiO <sub>2</sub>	SiO <sub>2</sub>	SiO <sub>2</sub>	SiN <sub>x</sub>	plasma passivation of p-GaN surface	SiO <sub>2</sub>
Aperture diameter	10 μm	8 μm	8 μm/ 10 μm	20 μm	7 μm	8 μm	10 μm
EBL	-/ 24 nm AlGaIn	-	-	p-AlGaIn	15 nm p-AlGaIn	20 nm p-AlGaIn	20 nm p-AlGaIn
InGaIn QWs/ GaIn Barriers	(10×) 2.5 nm/ 7.5 nm	(2×) 9 nm/ 13 nm	(5×)		(5×) 7 nm/ 5 nm	(5×) 5 nm/ 5 nm+ (1×) 10 nm B	(5×) Coupled 4 nm/ 4 nm
n-GaN thickness	790 nm/ 860 nm				902 nm	944 nm	
Cavity length	5λ*/7λ*	7λ*	about 4 μm	35λ	7.5λ	7λ*	13λ
Bottom DBR	(29×) AlN/GaN (SPSL)	(11×) SiO <sub>2</sub> / Nb <sub>2</sub> O <sub>5</sub>	(11×) SiO <sub>2</sub> / Nb <sub>2</sub> O <sub>5</sub>	SiO <sub>2</sub> / ZrO <sub>2</sub>	(13×) SiO <sub>2</sub> / Ta <sub>2</sub> O <sub>5</sub>	(42×) Al <sub>0.82</sub> In <sub>0.18</sub> N/SiO <sub>2</sub> / GaIn	(17.5×) SiO <sub>2</sub> / ZrO <sub>2</sub>
Substrate	sapphire	sapphire	GaN	GaN	GaN (m-plane)	GaN	sapphire
Substrate removal technique	-	laser lift-off and CMP	CMP	CMP	PEC	-	laser lift-off, ICP, and CMP
* The penetration depth into the DBR is not accounted for							

and GaN for the DBR design. The relative low refractive index contrast between these two compounds requires a large number of at least 46 and 54 pairs in the DBRs at 420 nm and 450 nm wavelengths, respectively. Both groups at NCTU and EPFL used a top DBR of dielectric material.

#### 3.2.2 Double dielectric DBR design

The problems with the epitaxial growth of high quality nitride DBRs might have tempted other groups to choose the double dielectric DBR route. Dielectric material with a large variation of refractive index is easily accessible and deposited with standard processes. The elimination of lattice matching criteria is another advantage

### 3.2. STATE-OF-THE-ART TECHNOLOGIES IN GAN-VCSELS

Table 3.2: Performance characteristics of electrically injected GaN-based VCSELs

	NCTU 2008/2010	Nichia 2008	Nichia 2009/2010	Panasonic	UCSB	EPFL	Xiamen
Emission wavelength (nm)	462.8/412	414.4	420/451/503	410	411.9	420	422
Maximum optical output power ( $\mu$ W)	-/37	140	620/700/800	3	19.5	300	0.5
CW/ pulsed	CW at 77K/ CW at RT	CW	CW/CW/ pulsed	CW	pulsed	pulsed	CW
Threshold current (mA)	1.4/9.7	7	1.5/1.5/22	2	70	70	0.93
Turn-on voltage (V)	4.1/4.3	4.3	-/3.3/6.3				4.3
Threshold like kink in IP characteristics	yes/yes	yes	yes/yes/yes	unclear	yes	yes	yes
Spectral linewidth narrowing above threshold (nm)	0.15/0.50	0.03	-	0.7	0.25	0.25	0.2

of this method. Extremely large high-reflectivity bandwidth can be obtained in the dielectric DBRs with fewer pairs thanks to their higher index contrast.

The significant challenge in this technique is to remove the substrate while maintaining a good control of the cavity length. There are a few approaches to remove the substrate. If the epi-layers are grown on sapphire, the substrate can be removed by laser lift-off and the rest of the GaN layers can be thinned down by means of chemical mechanical polishing (CMP). Inductive-coupled-plasma (ICP) etching could also be added to improve the flatness of the polished GaN surface [49]. However, many groups have recently used GaN substrates to improve the quality of the epitaxially grown layers. In this case, laser lift-off is not an option and the entire substrate is removed by CMP. The major problems are then the large inhomogeneity and poor thickness control associated with the CMP method, as described in Section 3.3. Therefore, researchers from UCSB have adapted a different way of substrate removal, namely bandgap selective photoelectrochemical (PEC) etching, which does not have the disadvantages of the CMP technique. The PEC etching and its benefits are also

Table 3.3: Material data at room temperature

Material	Refractive index at 420 nm	Lattice constant, $a_0$ ( $\text{\AA}$ )
AlN	2.18	3.112
$\text{Al}_{0.82}\text{In}_{0.18}\text{N}$	2.3	3.189
GaN	2.49	3.189

discussed in Section 3.3.

### 3.2.3 Intracavity contact schemes

So far, all schemes for electrical injection in GaN-based VCSELS are based upon an intracavity contact scheme, since the mirrors are non-conductive (undoped epitaxial DBR and dielectric DBR). The intracavity contact scheme is illustrated in Fig. 3.1, where the p-contact is deposited in a ring around the dielectric DBR stack and the n-contact as a ring on the n-GaN. To keep the lateral resistance low an n-GaN layer thickness of around  $1\mu\text{m}$  is required. How this thick n-GaN layer degrades device performance is explained in section 3.3. It can be mentioned that crack free n-type conductive DBRs have been demonstrated [52], but not yet implemented in VCSELS, partly due to the still high resistivity in those DBRs.

## 3.3 Additional challenges to be addressed

In order to improve the performance of GaN-VCSELS, a few more issues should be addresses besides the ones already mentioned in previous sections.

### Cavity length control

The cavity length of a VCSEL has to be precisely controlled to achieve not only a spatial overlap between the standing optical fields and the thin active region (i.e., the peak of the standing optical field has to be well-aligned to the position of the QWs), but also spectral matching between the material gain spectrum of the active region, the reflectance spectrum of the mirrors, and the resonance wavelength of the cavity.

In the case of double dielectric DBRs, it is difficult to control the length of the cavity with such precision, since one needs to remove the substrate and then deposit the backside dielectric DBR stack. The particular problem is with the chemical mechanical polishing (CMP) that is needed in this process to thin down the GaN substrate. The extreme uncertainty of the polishing process can lead to excess non-uniformity over a large area and therefore causing thickness and cavity length variations. The risk of losing the necessary aforementioned spectral and spatial overlaps can therefore increase significantly. In structures that are grown on sapphire at first laser lift-off is performed to separate the interface between the sapphire substrate and the GaN layer, and in order to prevent damaging of the QWs during the laser lift-off process, the GaN layer is usually grown very thick, which requires a CMP to thin it down eventually.

For these reasons, the approaches in which an epitaxial DBR is incorporated or the ones in which the substrate is removed using an alternative method such as a bandgap-selective photoelectrochemical (PEC) undercut etching are highly advantageous. By using an etch stop layer in the PEC etching the length of cavity can be controlled very precisely, but special attention has to be payed to the smoothness of the surface.

### n-GaN layer thickness

The use of intracavity contacts requires a not too thin n-GaN layer to keep the lateral resistance from the n-contact to the center of the VCSEL low. A typical thickness of the n-GaN layer is about  $1\ \mu\text{m}$ . Since this layer is doped the free carrier absorption, an optical absorption process, can be overall high for such a thick layer. Using the 2D effective index method explained in Chapter 4 we have calculated the threshold gain as a function of the absorption coefficient and n-GaN layer thickness, illustrated in Fig. 3.2b. Moreover, current transport simulations conducted by our partners at Politecnico di Torino show that the n-GaN thickness in a hybrid VCSEL scheme with a mesa-type intracavity contact can be reduced to about 500 nm and still avoid a too high resistance, as shown in Fig. 3.2a.

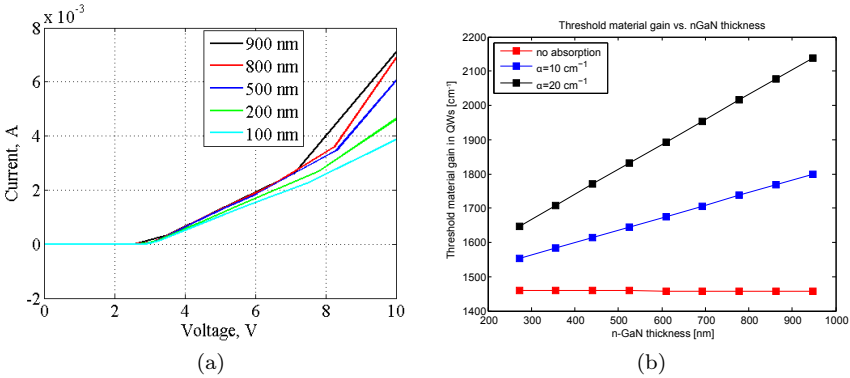


Figure 3.2: (a) Current-voltage curves for a mesa-type hybrid VCSEL obtained from APSYS simulations, with various n-GaN thicknesses. (b) Threshold gain values for the same VCSEL structure with various n-GaN thicknesses with different assumptions on the free carrier absorption coefficient  $\alpha$  of the n-GaN layer.

Another drawback with using a thick n-GaN layer is difficulty in controlling the absolute cavity length accurately. The effect of small variations in n-GaN thickness is illustrated in Fig. 3.3, which shows that the thickness of the n-GaN layer has to be controlled to within  $\pm 20\ \text{nm}$ .

### Long vs. short cavity

An alternative approach to trying to uphold the precise overlap between the gain spectrum, mirror reflectance spectrum, and cavity resonance wavelength is to make the VCSEL cavity longer to shrink the longitudinal mode spacing [46]. For a long cavity, the many longitudinal modes ensure that at least some always overlap with the material gain, and even when the gain spectrum shifts due to temperature effects some modes will still be lasing. This is the approach taken by a group at Panasonic. Of course, the optical losses in long cavity design can be larger and the threshold

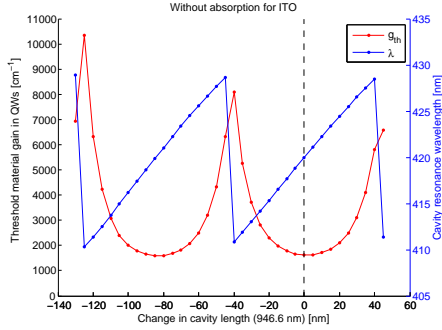


Figure 3.3: The effect on threshold gain and resonance wavelength of a small variation in the thickness of the n-GaN layer.

current to achieve lasing will not be the lowest possible. On the other hand, the threshold gain in long cavity design is less sensitive to fluctuations in cavity length, which can be large in case of CMP [53].

### Transparent contacts

To prevent current crowding due to the inefficient lateral current transport in the p-GaN layer, a transparent current spreading layer is used between the p-GaN and the DBR. The current spreading layer is made of indium-tin-oxide (ITO), an amorphous oxide with high lateral conductivity and optical (semi-)transparency. Thin films of ITO can be easily deposited on surfaces by physical vapor deposition techniques such as different types of sputtering, evaporation, etc.

In all of the GaN-VCSEL structures that have been realized so far ITO has been used as the transparent current spreading layer. Despite this wide usage, the properties of ITO are not ideal and has a direct negative impact on the device performance. The larger the ITO thickness, the better its conductivity, and the lower its transparency. Due to this trade-off, an ITO layer thickness thinner than about 30 nm is often used and it is placed in an optical field node of the VCSEL cavity to minimize the optical absorption.

Another problem arises due to the vulnerability of the p-GaN layer to plasma damage. This sets a limitation to the maximum plasma power that should be used for ITO deposition which can lead to increased porosity of the ITO film. In case of plasma damage, the contact resistivity between the ITO and p-GaN will be very high which can worsen the current injection and increase the heat generation in the device.

Some companies have mastered the ITO deposition on p-GaN surfaces [54, 55]. Although they do not reveal their exact process strategies it seems that they make use of a multi-layer ITO in which the first layers are more porous to avoid plasma

passivation of the p-GaN layer, and the upper layers are more dense for their increased conductivity.

There have also been many attempts to realize other types of transparent current spreading layers such as graphene [56], Al-doped ZnO [57], thin metal films [58], etc, mainly in GaN-based LEDs. So far ITO has shown the best performance in terms of electrical conductivity, contact resistance, and optical transparency. The research is still ongoing to find another material with better electrical and optical properties than ITO or to pursue a technological change in the structure so that a current spreading layer would not be needed anymore.

### Defects

The high density of defects in the epitaxial GaN layers can limit the optical and electrical performance in VCSELs. In DBRs, the defects and cracks can reduce the reflectivity and increase the scattering losses. In QWs, they can contribute to the increased rate of unwanted non-radiative recombination. Despite the high density of dislocations very high efficiency LEDs have been achieved, which has been attributed to the localization effects, in which the dislocations sites are screened and have a reduced impact [59, 60]. Adding to the problems, dislocations can form current leakage paths, making the realization of effective current injection much more challenging. By using GaN substrates instead of sapphire, devices with better performance are expected thanks to the lower defect density [44].

### Temperature effects

The short lifetime of the GaN VCSELs can be attributed to the high resistivity of the ITO/p-GaN contact and the large self-heating that in general prevent the devices from CW lasing. The heating effects may not only modify the guiding properties of the cavity (see Chapter 4), but can also decrease the optical material gain in the QWs, as well as reducing the modal gain since the spectral overlap between the gain peak and the resonance change with temperature. It can also destroy the ITO/p-GaN contact if contact resistivity is high. Since in VCSELs a high current density is often required, the current crowding effect can induce an increase in the operating voltage and heat generation. Thus, efficient heat dissipation capabilities through the substrate is highly essential to reduce the temperature effects. Devices grown on sapphire substrates, which have a poor thermal conductivity, may therefore not be preferred. Also if a double dielectric scheme is used, a vertical structure in which the bottom dielectric DBR is decreased to a small area has a better performance since most of heat can be removed through the metal bonding. In [46], the cavity is designed to be very long ( $35\lambda$ ) so that the longitudinal mode spacing becomes very short. In this way, many modes overlap with the optical gain spectrum and the effect of temperature induced gain shift would be reduced, although the problem with the reduced QW material gain still remains.

#### **Lateral current and optical confinement schemes**

It is essential to confine both the current and the optical field laterally to the center of the VCSEL to increase the overlap between gain and optical field, and to be able to achieve the high threshold current densities required for lasing, typically  $10 \text{ kA/cm}^2$ . The confinement technique that is widely used in GaAs-based VCSELS, to make an oxide aperture is not easily implemented in GaN-based materials. Therefore, different groups have tried to form an aperture between the p-GaN and the ITO, mostly by using a low index dielectric material that blocks the current, and opening a hole in its center to pass the current through. However, this scheme results in a non-planar structure that is depressed in the center, i.e., has a downward step profile. We have investigated the optical properties of such cavities in terms of guiding properties and losses using our in-house developed VCSEL simulation tools that are based on the effective index method (EIM) and 3D coupled-cavity beam propagation method. We found that the non-planar centrally depressed structures yield an anti-guided cavity with associated high losses. The work regarding this topic is explained in further details in Chapter 4.

# Chapter 4

---

## Guiding/Antiguinding effects in GaN-based VCSELs

---

Achieving a high enough current density to enable lasing obliges us to introduce an aperture to confine the current to the central part of the device. However, the aperture changes the optical properties of the laser cavity, both because the cavity structure changes and because the confined current changes the temperature distribution. This chapter describes these effects, how they can be modeled, and the strong impact they can have on the laser performance.

Definition of apertures in GaN-based light emitting devices have so far been divided mainly to three main schemes: (1) dielectric  $\text{SiN}_x$  or  $\text{SiO}_2$ ; (2) epitaxial AlN [61, 62] and AlInN [63] aperture using regrowth; (3) oxide aperture through selective oxidation of AlInN [64]. In schemes (1) and (2), the transverse current confinement is obtained by deposition of an electrically non-conducting layer and then making an opening (a few micrometer in diameter) in the center to pass the current through. The surface of the resulting structure is no longer planar i.e. has a negative (downward) step profile, which is also referred to as having a depression in the structure, see Fig. 4.1a. In scheme (3), a continuous AlInN layer is grown in between the p-GaN layers and it is then selectively oxidized from the mesa sides. In this case, the surface of the structure will be planar and flat provided the oxidation does not lead to strong expansion or contraction of the oxidized material.

Most of the groups working on GaN-based VCSELs [41, 42, 46, 47, 49] have employed only scheme (1), probably due to the difficulty of controlling the oxidation and/or the regrowth in schemes (2) and (3). The only exception is the work by Cosendey and coworkers at EPFL [48], in which the transverse current confinement is obtained using p-GaN surface passivation by reactive ion etching (RIE) with an Ar/ $\text{CHF}_3$  plasma. The RIE treatment slightly etches material outside the aperture region so that the top surface of the structure has a shallow elevation of about 10 nm in the center, see Fig. 4.1b.

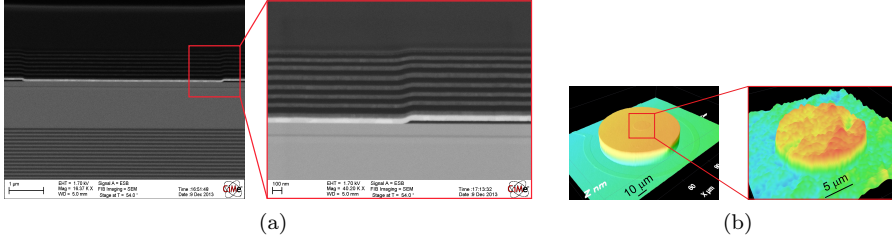


Figure 4.1: (a) Central depression of the top surface in a device with SiO<sub>2</sub> aperture. (b) Central elevation of the top surface in the device with RIE-treated GaN.

As will be shown the degree of depression or elevation of these non-planar structure is simply and directly related to the ability of the laser cavity to work as a good waveguide. This is of great importance in efficient operation of semiconductor lasers by providing a better overlap between the photons and the charge carriers and reducing excessive transverse radiation loss. This is reached when the effective index of the structure at the center of the device is higher than the one in the periphery. In the case of structures with depression in the center, the layers that are deposited after the formation of the aperture (e.g. ITO layer and dielectric DBR) will basically follow this form having a depression equal to the thickness of the aperture layer. However, in such non-planar multi-layer structure there will be some cross-sections in which the refractive index of the material in the periphery is larger than that of the central part, as shown by the red dashed lines in Fig. 4.2. There is therefore a large risk that if the standing optical field is strong at these cross-sections, the overall device will act like an anti-guided structure. An anti-guided structure will lead to a higher lateral radiation loss and thereby higher threshold currents and lower output powers, if lasing at all is possible.

## 4.1 Optical guiding study

In order to theoretically investigate the behavior of the cavities with different planar and non-planar structures, a numerical simulation model based on a quasi-two-dimensional (2D) effective index method (EIM) was applied to calculate the cold-cavity index guiding,  $\Delta n_{eff}$  values [65]. The  $\Delta n_{eff}$  parameter depends on the cavity structure and the modal field distribution. It is a very reliable indicator of the cavity's ability to guide the light and prevent lateral loss, as will be shown. The EIM can also provide accurate threshold gain values for every transverse mode if the structure is weakly positive index guided, i.e.,  $0 < \Delta n_{eff} < 0.03$ . Under such conditions, the lateral radiation loss is negligible. In other cases, i.e. for strong positive guiding and negative guiding (anti-guiding), another model based on a three-dimensional (3D) Beam Propagation Method (BPM) was used with substantially longer computation time, but accounting for lateral radiation loss mechanisms including diffraction and lateral leakage, the latter which signifies the excessive lateral loss that occurs in antiguided cavities [66].

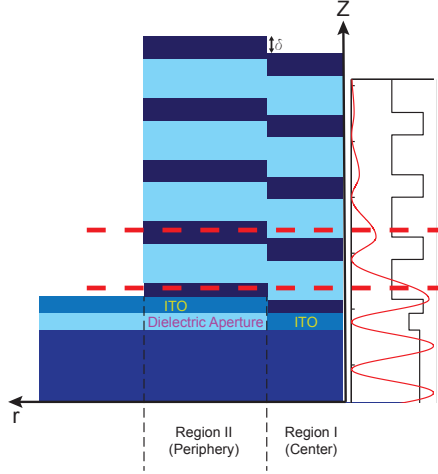


Figure 4.2: Schematic illustration of part of the VCSEL structure where the introduction of an aperture has resulted in a depression in the central part. At the cross-sections shown by red dashed-lines the refractive index in the periphery is larger than in the center, which can possibly lead to antiguiding. Also shown is the refractive index profile at the center of the device and the amplitude of the optical field along the symmetry ( $z$ -)axis.

Using the 2D-EIM model described in [65], the  $\Delta n_{eff}$  value is calculated by performing a 1D-simulation in the center of the structure and another one in the periphery (where the aperture is incorporated). From each of these runs, a list of different parameters are calculated such as: cavity resonance wavelength,  $\lambda_0$ , threshold material gain in QW,  $g_{th}$ , variation in the real part of the effective dielectric constant,  $\Delta Re(\epsilon_{eff})$ , weighted dielectric constant,  $\langle \epsilon \rangle$ , cavity quality factor,  $Q$ , among others. The index guiding value is then calculated as,

$$\Delta n_{eff} = \frac{\Delta Re(\epsilon_{eff})_{center} - \Delta Re(\epsilon_{eff})_{periphery}}{2 \times \sqrt{\langle \epsilon \rangle}}, \quad (4.1)$$

Figure 4.3 illustrates the standing optical fields that are obtained for a VCSEL structure in two regions. Region I is the center of the device inside the aperture and region II is in the periphery of the device where a dielectric  $\text{SiO}_2$  exists between the p-GaN and the ITO layers.

#### 4.1.1 Hot-cavity: The effect of self heating

A realistic investigation of GaN based lasers under operation should in principle include the significant temperature rise inside the cavity. Large self-heating occurs in

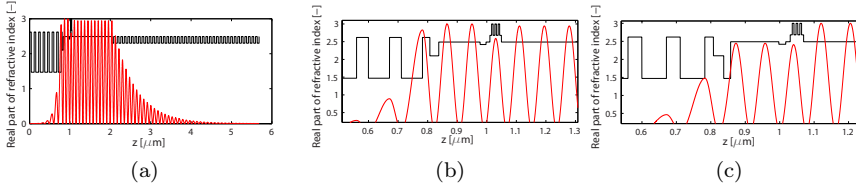


Figure 4.3: Longitudinal profiles of the refractive index (black) and standing optical field (red) in a VCSEL structure. (a) Region I, which is the center of the device, (b) zoom-in of region I (c) zoom-in of region II, which is the periphery of the device. (Note the low-index SiO<sub>2</sub> aperture between the p-GaN and ITO.)

the cavity since the required injected current densities and the existing internal resistances are both high. Self-heating in current driven devices can have a large impact on the optical properties of the device due to the temperature-induced change in the refractive index. Besides, the bandgap of semiconductors shrinks with temperature. Therefore, it was well justified to extend the previous simulations by including the temperature effects. This was particularly motivated by the observation that even small variations in structure, i.e., refractive index, could lead to large variation in the optical properties.

The temperature study started with a current transport simulation, performed by our collaborators in Politecnico di Torino, for reasonable working voltages. The results of their simulation are presented in Fig. 4.4. They are used to calculate the spatially varying internal Joule heating  $Q_J$ ,

$$Q_J = \frac{\vec{J}_n^2}{\sigma_n} + \frac{\vec{J}_p^2}{\sigma_p}, \quad (4.2)$$

where  $\vec{J}_n$  and  $\vec{J}_p$  are the electron and hole current densities and  $\sigma_n$  and  $\sigma_p$  are their respective conductivities. Solving the heat transfer equation with the calculated Joule heating, the 2D temperature distribution was obtained, which is shown in Fig. 4.5.

The next step was to incorporate the temperature distribution curves into the 2D optical model and redefine the effective refractive index changes which originate from the temperature-induced change of the refractive index in the materials. For this, tabulated values for the thermo-optic coefficients of the cavity materials were used. The modified effective index distribution due to the self-heating is illustrated in Fig. 4.6.

The same temperature effects have also been incorporated into the 3D optical model based on BPM, thus likewise modifying the refractive index distribution, after which the losses and the threshold material gains were calculated in the same manner as in the cold-cavity case. The final results are presented in paper C.

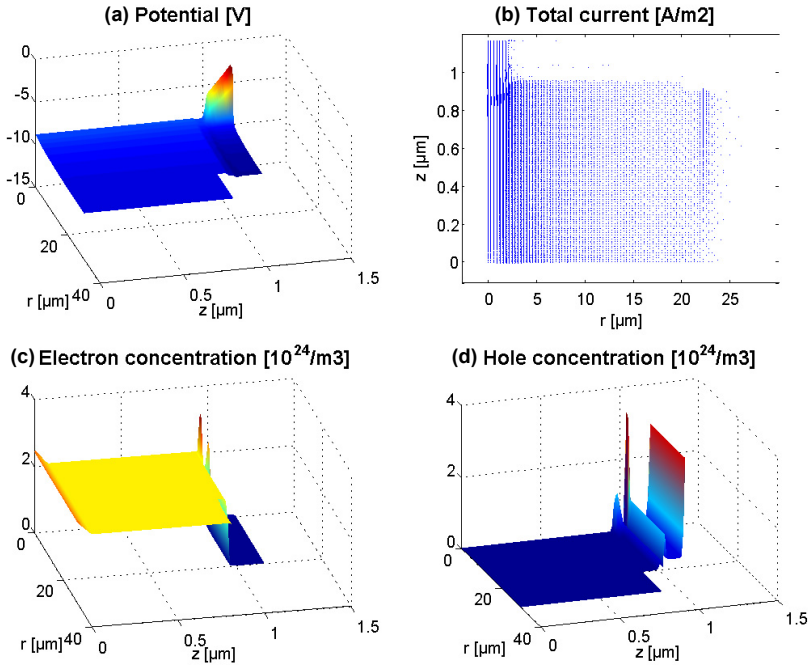


Figure 4.4: Current transport simulation results using APSYS software, under drive conditions of 10 V potential (corresponding to  $\sim 8$  mA total current).

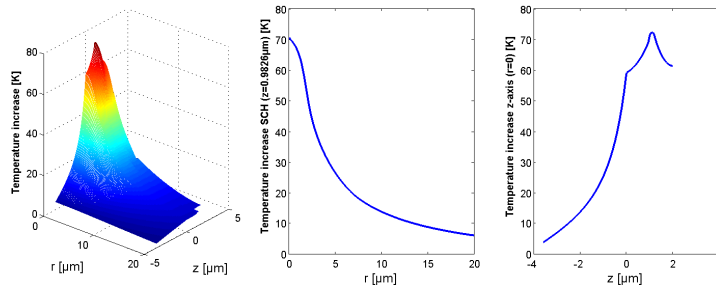


Figure 4.5: Temperature distribution (from Joule heating) in the cavity, and temperature profiles in two representative horizontal and vertical cross sections.

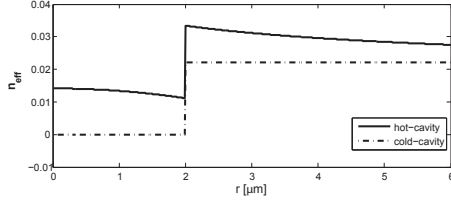


Figure 4.6: Change of index guiding value  $n_{eff}$  due to temperature induced refractive index change.

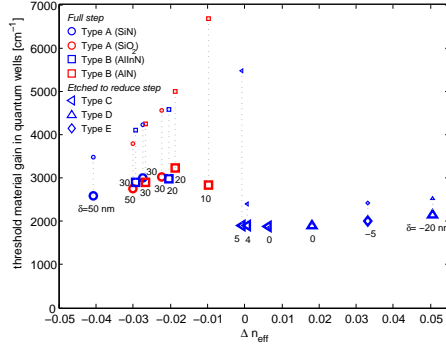


Figure 4.7: Calculated threshold gain for the fundamental mode in the different laser cavities. Large markers are for cold-cavities, whereas the corresponding smaller markers indicate the results when thermal lensing is included. The structural depression parameter  $\delta$  is shown with negative numbers for elevated structures. Type A–E are the structural types of laser cavities shown in paper B and C.

## 4.2 The main conclusions

Figure 4.7 shows the threshold gain values for a large number of simulated cavities, both cold-cavity and with self-heating included, as functions of  $\Delta n_{eff}$ . Also indicated is the profile step  $\delta$  of the cavity structure. It is evident from the figure that  $\Delta n_{eff}$  is a very good measure of the waveguiding ability of the cold cavity ( $\Delta n_{eff}$  is a property of the cold cavity for every structure), with  $\Delta n_{eff}=0$  making the border between antiguided, high threshold, and guided, low threshold, regimes. The figure together with other results from the simulations enable some important conclusions to be drawn.

- The guiding character of GaN-VCSELS can change strongly even for very small structural changes.
- The transition region between the guiding and the anti-guiding should be avoided due to the very high lateral losses.

- Cavities with fairly strong antiguiding have
  - Higher threshold gain than guided cavities, which further is temperature dependent and decreases with increased self-heating.
  - Built-in modal discrimination that is largely insensitive to self-heating.
- Cavities in guided regime have
  - The lowest threshold gain, which further does not depend at all on self-heating.
  - Lack of modal discrimination (can possibly be obtained with e.g. shallow surface structures).
- As a simple design guideline, thus, antiguided structures should be avoided to minimize the threshold gain, even if the strongly antiguided regime might be of interest with its moderate threshold gain and strong favoring of the fundamental mode.



# Chapter 5

---

## High contrast grating reflectors for GaN-based VCSELs

---

The behavior of optical gratings is easy to predict if the grating period,  $\Lambda$ , is either much larger or much smaller than the wavelength,  $\lambda$ . But because of resonance effects the behavior of gratings in the near-wavelength regime,  $\Lambda \approx \lambda$ , is found to be extraordinary, especially when the refractive index contrast is large. In 2004, Hasnain and coworkers proposed the idea of high contrast gratings (HCGs) and experimentally realized a surface-normal reflector with more than 99% reflectance and a high-reflectance bandwidth  $\Delta\lambda$  as large as  $\Delta\lambda/\lambda > 30\%$ . Since then the field has rapidly expanded with both experimental demonstrations and theoretical explanations for the spectacular reflectance properties of HCGs. Among different suggested applications of HCGs, using a HCG as the top reflector in a VCSEL has drawn major attention. HCGs as VCSEL mirrors are believed to have several unique inherent advantages compared to the already well-established DBRs, such as broadband reflectivity, polarization selectivity, wavelength setting capability for multiple-wavelength VCSEL array, transverse mode control for single-mode devices, improved tuning speed and range for tunable VCSELs, among others.

### 5.1 Structural description

The schematic of a part of HCG structure is illustrated in Fig. 5.1, assuming an infinite number of grating beams which are infinitely long, or at least that the grating extends far beyond the area illuminated by the incident light beam. The grating structure has a thickness of  $t_g$ , width of  $\omega$ , and period of  $\Lambda$ . The duty cycle or the fill factor is defined as the ratio  $\omega/\Lambda$  between the grating beam width and the period. The grating material is normally chosen to have a high refractive index of  $n_g$ , which is surrounded by a low index material  $n_l$ , preferably air, which has the lowest index.

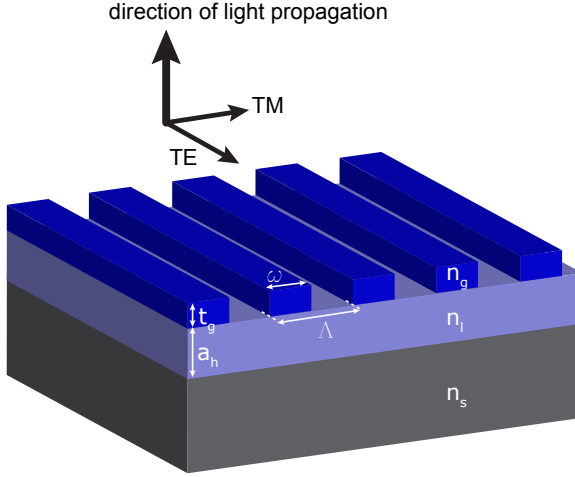


Figure 5.1: Schematic of HCG with a high index grating material ( $n_g$ ), low index material ( $n_l$ ), and substrate index ( $n_s$ ). HCG parameters are the layer thicknesses  $t_g$  and  $a_h$ , period  $\Lambda$  and duty cycle  $\omega/\Lambda$ .

In the case of having an air-suspended HCG, i.e., grating beams entirely surrounded by air, the parameter  $a_h$  is referred to as the airgap. The two polarizations of a normally incident plane wave, transverse-electric (TE) and transverse-magnetic (TM), are defined in the direction along and perpendicular to the grating beams, respectively, as shown in the figure.

The fundamental working principles of HCGs have been explained and analytical formalisms have been published, which are reviewed thoroughly in [67]. A simplified intuitive picture can be obtained by first considering a conventional grating with large features,  $\Lambda \gg \lambda$ . When a normally incident plane wave is exposed to the grating structure, it can diffract into many directions, depending on the grating period and the wavelength. However when  $\Lambda$  shrinks to values near  $\lambda$  only the 0-th diffraction order can carry significant energy, either in reflection or transmission. If the parameters of the grating are designed properly, e.g. the grating thickness is set such the accumulated phases of the waves passing through the grating beams and the air spacing in between them allow for a destructive interference at the output plane, the optical power will be launched back to the low index medium and thus reflectivity will, in theory, be equal to unity.

## 5.2 Application of HCGs in VCSELS

Up to now, only a few electrically-pumped HCG-VCSELS have been realized, and mainly for infrared wavelength regime. Among these there are three examples where the HCG is incorporated as part of the top reflector in combination with a few DBR

pairs, at 850 nm [68], 980 nm [69], and 1550 nm [70] wavelength, using AlGaAs/air, GaAs/oxide, and InP/air HCGs, respectively. However it was shown in two other experiments that the top DBR can be completely substituted by a HCG with high enough reflectivity, in devices employing GaAs/air HCG at 1060 nm [71] and Si/SiO<sub>2</sub> HCG at 1320 nm [72] wavelength. One should also mention an optically pumped VCSEL using two HCGs as the top and the bottom reflectors, which proves the concept of DBR-free VCSELs [73].

Thus there are hopes that HCGs can be a solution for one of the key challenges in GaN-based VCSELs at blue-green emission wavelengths [11], the realization of high quality feedback mirrors. This is very demanding in GaN-based DBRs due to relative small index-contrast and/or the large lattice mismatch in this material system. In addition to the high reflectivity and wide reflectivity stopband, HCGs can offer post-epitaxy wavelength setting, which can be desirable for GaN-VCSELs suffering from growth inhomogeneities.

Some groups have consequently attempted to realize III-nitride membrane type HCG structures for the visible regime, in spite of difficulties in this material system to obtain wet etch selectivity in a simple way. For instance, bandgap-selective photoelectrochemical (PEC) etching of InGaN superlattice layers has been performed to make AlGaIn gratings, but with limited airgap height [74], or a focused-ion-beam (FIB) etching process was employed to drill a large airgap underneath a GaN grating pattern [75]. In addition, GaN HCGs using GaN-on-Si have been demonstrated by backside Si wafer etching [76, 77], however the integration to VCSELs will be very difficult since high enough quality growth of epi-on-Si is still extremely challenging. Due to this technological problem, Lee et al. [78], have proposed a GaN grating reflector with no airgap. Although this scheme is more mechanically rigid, the fabrication tolerance for reflectivities higher than 99% will be much smaller, suggesting that the air-suspended type should be preferred. Another example with no air-suspension is an optically pumped GaN-based VCSEL using a photonic crystal HCG [79], in which the grating pattern (an array of beams) is drilled down to about 0.5  $\mu\text{m}$  through the multiple quantum wells.

In this chapter, the details about design and fabrication of a free-standing dielectric HCG suitable for the visible regime, made of TiO<sub>2</sub> material, are discussed. Among the dielectrics, TiO<sub>2</sub> has a high refractive index of about 2.6, similar to that of GaN, with a negligible absorption for wavelengths longer than 400 nm. As a dielectric sacrificial-etch layer SiO<sub>2</sub> is suitable, providing an extremely high wet etch selectivity. This scheme leads to a robust way of direct integration to different material systems since the lattice matching is not a prerequisite and the residual stress in the dielectric films can be tailor-made to a value that, in the end, yields grating beams that do not buckle or bend.

### 5.3 Fabrication of TiO<sub>2</sub>/air HCG

The fabrication steps of the TiO<sub>2</sub>/air HCG are summarized schematically in Fig. 5.2. In our case, the as-deposited TiO<sub>2</sub> films using the standard deposition parameters resulted in very good optical (high refractive index and low absorption) and chemical

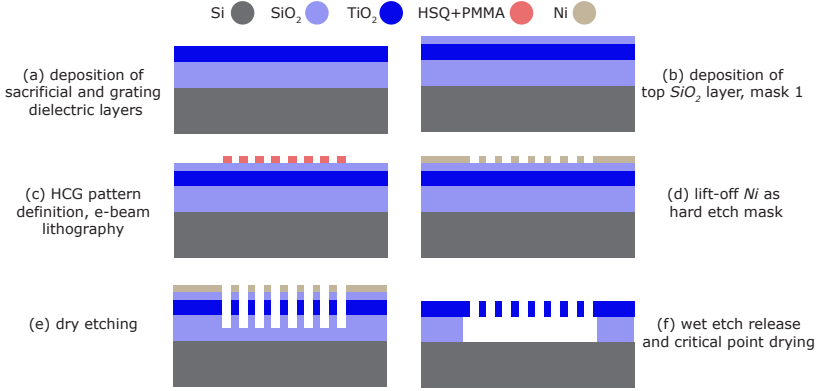


Figure 5.2: Schematic of HCG fabrication steps.

(high wet-etch selectivity) properties, but the mechanical residual stress had to be modified. This modification in the deposition parameters led to different dry etching behavior by the film, so thereby the process parameters of the dry etching had to be optimized as well. Moreover, both the residual stress and the dry etching behavior significantly depended on an optional annealing process. This interplay and mutual dependence between the processes were the main challenges of this work.

### 5.3.1 Dielectric stack deposition

The first step in the fabrication is the deposition of the dielectric stack. As it can be seen in Fig. 5.2, in addition to the SiO<sub>2</sub> and the TiO<sub>2</sub> layers that serve as the sacrificial and the grating layers, an extra SiO<sub>2</sub> layer is also used to improve the dry etching profile of the grating TiO<sub>2</sub> gratings. The fabrication details of the dielectric stack are summarized in Table 5.1. The SiO<sub>2</sub> deposited by PECVD was thought to be less dense and thus more suitable for wet etch removal. The sputtering was the only method available for TiO<sub>2</sub> deposition, where the use of RF bias power could be varied to modify the residual stress of the film.

### 5.3.2 Annealing

Annealing the dielectric stack at this stage can alter the properties of the films. For example the dry etching behavior of the TiO<sub>2</sub> film can be improved since the film gets denser and therefore sharper sidewalls can be achieved more easily. However, due to the increase of the tensile stress in the TiO<sub>2</sub> film during annealing, it was decided to skip this step, which to some extent made the dry etching optimization a more challenging process.

Table 5.1: Fabrication details of the dielectric stack

No.	Process step	Tool	Process parameters
1	bowing (stress) measurement on 2-inch Si substrate	Tencor surface profilometer	-
2	SiO <sub>2</sub> deposition	PECVD-Oxford plasmalab 100 system	standard recipe
3	bowing (stress) measurement after deposition	Tencor surface profilometer	-
4	TiO <sub>2</sub> deposition	Sputtering-FHR MS150	1 kW dc power, $5 \cdot 10^{-3}$ mbar, 40 sccm Ar flow, 12/4 sccm O <sub>2</sub> flow, 300–400 W RF bias power
5	bowing (stress) measurement after deposition	Tencor surface profilometer	-
6	SiO <sub>2</sub> deposition	Sputtering-FHR MS150	1 kW RF power, $1.2 \cdot 10^{-2}$ mbar, 40 sccm Ar flow, 15 sccm O <sub>2</sub> flow

### 5.3.3 Pattern definition and Ni lift-off

The patterns that are designed for the HCGs were defined on the sample using an electron beam (e-beam) lithography. A bilayer negative e-beam resist made of the combination of hydrogen silesquioxan (HSQ) and poly-methyl-methacrylate (PMMA-A2) was utilized as it has proven well suited for the subsequent Ni lift-off process [80]. 50 nm thick Ni was evaporated onto the developed resist using an e-beam evaporation system followed by lift-off to create the required hard mask for the etching process.

### 5.3.4 Dry etching

The full description of the dry etching is in Paper D. In brief, the metal-oxides are etched with fluorine based gases, among which CHF<sub>3</sub> has the advantage of forming controlled amount of fluoro-carbon polymers that can help protecting the side walls. With the right amount of CHF<sub>3</sub> and the right value of the plasma power good directionality can be obtained. We found out that by having a low pressure (<5 mTorr) and certain amount of electrode RF power (75 W) and ICP power (125 W) we can control the etch rate and the directionality of the etching in a way that sharp edges of TiO<sub>2</sub> grating can be obtained, even when the dielectric films are not annealed previously.

After etching the cross-sections of the gratings were characterized using Scanning Electron Microscopy (SEM) to control not only the side walls of the grating but also to ensure that the etch had been continued deep into the bottom SiO<sub>2</sub> layer. With a too shallow etch into the bottom SiO<sub>2</sub> layer would make the following wet etch removal of the sacrificial layer more difficult and time consuming.

### 5.3.5 Wet etch sacrificial removal

The Ni hard mask was first removed using a Cr/Ni wet etch solution. In order to ensure that the Ni is entirely removed, the samples were submerged in the 60°C-Cr/Ni solution for at least 15 minutes. After that the critical wet etch removal of the SiO<sub>2</sub> layer was performed utilizing a diluted mixture of Buffered-Oxide-Etch (BOE) and water with a 1:5 ratio for 4 minutes to selectively etch away the SiO<sub>2</sub> and release the grating structures. Finally the samples had to undergo a critical point drying step so that they do not bond to the substrate by the capillary forces.

## 5.4 Characterization of TiO<sub>2</sub>/air HCG

The fabricated HCGs are small, their diameters often  $<20\mu\text{m}$ , and designed for normal incident reflection. This makes the characterization and reflectivity measurement of the HCGs a very challenging task. The incoming light must have a spot size less than the diameter of the HCG, and impinge on the grating surface with a normal angle. Therefore, lenses are used to focus the incoming light down to the desired size. However, in this case, the numerical aperture of the lens determines the range of the angles within which the incoming light hits the grating surface. In such case, a narrow pinhole has to be used to limit the acceptance angle as much as possible.

As the schematic in Fig. 5.3a presents, a micro-reflectance measurement setup was used to evaluate the optical performance of the realized HCGs. In this setup incoming light from a Xe white light source is tightly focused with a lens, a pinhole with a circular aperture, and a microscope objective (100 $\times$ , numerical aperture=0.5) to a spot size of about 5–10  $\mu\text{m}$  on the grating, as the diameter is only 12  $\mu\text{m}$  for the characterized gratings. Another aperture with 1.5 mm minimum opening is placed beneath the objective at a distance of 7 mm to the sample to limit the acceptance angle of the incident and collected light. The acceptance angle in horizontal direction is defined by this aperture ( $-6^\circ < \theta_\perp < +6^\circ$ ), while the acceptance angle in vertical direction is defined by the 300  $\mu\text{m}$  narrow entrance slit of the spectrometer ( $\theta_\parallel < \theta_\perp$ ). Moreover, a polarizer is inserted in the light path to allow for characterization of the polarization selectivity of the HCG.

In order to define the absolute reflectance (or the 0-th order reflected diffraction efficiency, to be precise) value, the spectrum acquired from the HCG is divided by the reflectivity of the Al reference mirror. However, the obtained value will be overestimated due to the fact that Al has a reflectivity of only  $\sim 90\%$  in the visible spectrum. Therefore, by measuring the reflectivity of the bare TiO<sub>2</sub> surface adjacent to the grating (region 2 in Fig. 5.3b) and comparing it with its numerically simulated reflectivity spectrum we can easily estimate an almost wavelength independent normalization factor of 1.2 that accounts for the imperfect reference. The measured spectrum from the grating is then divided not only by the Al reference mirror reflectance but also by the normalization factor to realistically calculate the absolute values for the reflectance spectrum. This is schematically illustrated in Fig. 5.3b. Fig. 5.4 contains the extracted reflectance spectra for both TM and TE polarization. Peak reflectance values exceeding 95% near the center wavelength of 435 nm with a full-width at half-maximum (FWHM) for the stopband of about 80 nm are achieved

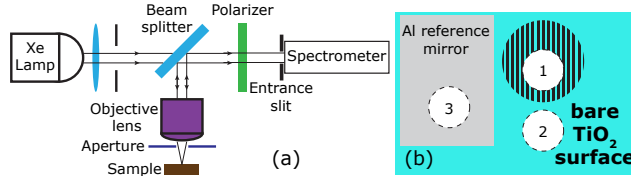


Figure 5.3: (a) Schematic of the micro-reflectance setup. (b) For calculating the absolute reflectance three reflectance spectra were captured in the regions on the sample indicated by circles, the sizes of which roughly indicate the diameter of the incident light beam; region 1 on the grating; region 2 on the adjacent bare TiO<sub>2</sub> surface; and region 3 on the Al reference mirror.

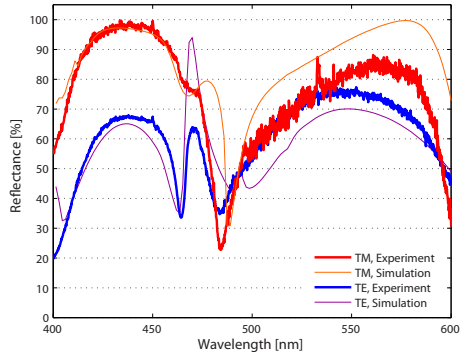


Figure 5.4: Measured and simulated reflectance spectra of the TiO<sub>2</sub>/air HCGs for both the TM- and TE-modes.

for the TM polarization. The peak reflectance for the TE polarization is however only 30% lower which is a much smaller difference than the theoretical predictions indicate. This is because it is not possible to isolate the reflectivity from the HCG from that of the structure beneath. The HCG is poorly reflective for the TE polarization and therefore much of the reflection comes from the underlying Si substrate. Including the Si substrate in the RCWA simulation, the numerical results reproduce the measured reflectivity spectra very well when a finite acceptance angle of  $6^\circ$  is accounted for in the simulation model by averaging the reflectance values for different angles of the incoming light. In this simulation the refractive index dispersion of TiO<sub>2</sub> is incorporated from the earlier measured ellipsometry data.



# Chapter 6

---

## Future outlook

---

The future for the GaN-based VCSELs can be very bright thanks to the applications that are expectable or maybe still unforeseen. In such cases, the history can always be a good guide. The history of technological developments of GaAs-based VCSELs were outlined briefly in the introduction chapter, starting with the first demonstrations by Iga in 1977. However, it is noteworthy to mention that Honeywell (later acquired by Finisar Co.) commercialized them first in 1995, showing the time and the effort it usually takes from a demo to a reliable high-performance device. The fact that two big companies (Nichia Co. and Panasonic) have put so much effort in blue GaN-based VCSELs indicates that they believe that there is a big commercial value in this field. In addition to this, the increased number of research groups that have demonstrated lasing action during recent years, and the increased number of contributions at conferences such as SPIE Photonics West 2015 show the interest this field has arisen. It is expected that many more applications for UV-blue-green microcavity lasers and RCLEDs appear once such light sources actually exist.

The prospects of the GaN-based VCSELs and the future directions depend mostly on the understanding of the challenges and the shortcomings of the current technologies. Based on the challenges that were explicitly introduced in chapter 3, we can identify some possible outlook and future work for the electrically pumped GaN-based VCSELs, such as the following.

### ITO replacement

As explained earlier, the suboptimal performance of the ITO current spreading layers is one of the main issues of the current technologies. The ITO technology has been pushed to its performance limits, so further progress seems to rely upon either new materials for a transparent current spreading layer or new current injection/spreading schemes. So far, most of the alternative materials proposed to replace ITO have

unfortunately failed to outperform ITO, including highly transparent 2D materials such as graphene. On the other hand, very recently low-resistance tunnel junctions in the GaN material system have been demonstrated using strained InGaN [81], Gd-nano islands [82], and highly doped GaN [83]. This is very promising, since by replacing the p-GaN with higher conductivity n-GaN there would be no need for an additional current spreading layer such as ITO, and low-resistive contacts would be easily achieved [11].

### **GaN-on-ZnO epitaxy**

The similar wurtzite structure and the small 1.9% lattice constant difference between ZnO and GaN make the heteroepitaxy of these materials very interesting [84]. For example, high quality multilayer stack of ZnO and GaN layers grown on top of each other can be promising in DBR application at blue-green spectral regions. The high wet etch selectivity between these two materials [85] can be practically implemented to make ZnO sacrificial layers to either make free-standing GaN HCGs, or be used as a way of substrate removal in a double dielectric DBR scheme.

### **Conductive DBRs**

So far all of the DBR schemes used in the GaN-based VCSELs are nonconductive (undoped semiconductors or dielectric materials). There has been one demonstration [52] of conductive n-type DBRs in the GaN-based material technology, if implemented in VCSELs, this can be extremely useful and improve the device properties. In such case, the cavity can be made much shorter since no intracavity contacts will be needed for the n-side of the active region, and the n-GaN thickness can be reduced significantly. The lateral current transport may also be improved. Moreover, such scheme can possibly have an improved heat dissipation capability and enhance the cw operation of the devices.

### **Nonpolar m-plane GaN substrates**

Lastly, the non-polar and semi-polar orientations have the potential to yield an increased optical gain and thereby lead to reduced threshold current. Non-polar and semi-polar orientations might as well enable arrays of polarization-stable VCSELs [86].

# Chapter 7

---

## Summary of Papers

---

### Paper A

**"Engineering the Lateral Optical Guiding in Gallium Nitride-Based Vertical-Cavity Surface-Emitting Laser Cavities to Reach the Lowest Threshold Gain"**, *Jpn. J. Appl. Phys.*, vol. 52, no. 8S, pp. 08JG04, May 2013.

In this paper we show, by using a two-dimensional (2D) effective index method and a three-dimensional (3D) coupled-cavity beam propagation method, that the scheme employed by most groups in order to confine the current using a dielectric aperture typically results in optically antiguided structures with high optical losses and thus very high threshold gains. It was also observed that the threshold gain notably reduces with increased negative guiding. Nevertheless, moderately positively guided designs are proposed to be implemented to avoid the detrimental effect of lateral leakage and high diffraction loss, by flattening the structure or even introducing an elevation near the optical axis by additional processing. The associated threshold material gain are estimated to reduce from 6000 to 2000  $\text{cm}^{-1}$  for the studied structures.

### Paper B

**"Analysis of structurally sensitive loss in GaN-based VCSEL cavities and its effect on modal discrimination"**, *Opt. Express*, vol. 22, no. 1, pp. 411–426, Jan. 2014.

In this paper we further analyzed the cold-cavity of the antiguided and guided structures by estimating the contributions of outcoupling (mirror) loss, material absorption, and lateral loss to the total loss in proposed GaN-based VCSELs. The lateral

loss was extremely sensitive to small structural changes. Moreover, it was found that modal discrimination in the antiguided regime was not as strong as the prediction had suggested. Nonetheless, our simulations indicated a moderate 50-100% increase in lateral leakage loss for the first higher order mode compared to the fundamental mode.

### Paper C

**"Triggering of guiding and antiguiding effects in GaN-based VCSELs"**, *Proc. SPIE, Vertical-Cavity Surface-Emitting Lasers XVIII*, vol. 9001, 90010A, Feb. 2014.

This conference paper is the extension of the previous papers by including the self heating effects on the guiding properties of the antiguided and guided cavities. Similarly as before, the threshold material gain and modal discrimination were calculated for the cavities and the results between the cases, with and without including the temperature effects, were compared. It was shown that thermal lensing caused by device self-heating under operation can dramatically reduce the optical loss but not the modal discrimination in the antiguided cavities.

### Paper D

**"TiO<sub>2</sub> membrane high-contrast grating reflectors for GaN-based vertical-cavity light emitters"**, *Submitted to Applied Physics Letters*.

This letter is a report of our experimental investigation of an alternative method to realize a high-contrast grating structure for blue emitting GaN based VCSELs using air-suspended TiO<sub>2</sub> gratings with a SiO<sub>2</sub> sacrificial layer. Design, fabrication, and optical characterization of the gratings are outlined in this paper. A peak reflectance exceeding 95% is achieved with a FWHM of 80 nm and a good agreement between simulated and measured reflectivity spectrum is shown.

---

## References

---

- [1] A. Haglund, J. S. Gustavsson, J. Vukusic, P. Modh, and A. Larsson, "Single fundamental-mode output power exceeding 6 mW from VCSELs with a shallow surface relief," *Photonics Technology Letters, IEEE*, 16(2):368–370, 2004.
- [2] D. Kuchta, A. V. Rylyakov, C. L. Schow, J. Proesel, C. Baks, P. Westbergh, J. S. Gustavsson, and A. Larsson, "64Gb/s Transmission over 57m MMF using an NRZ Modulated 850nm VCSEL," In *Optical Fiber Communication Conference*, pages Th3C–2. Optical Society of America, 2014.
- [3] P. Westbergh, J. Gustavsson, and A. Larsson, "VCSEL Arrays for Multicore Fiber Interconnects with an Aggregate Capacity of 240 Gbit/s," *Photonics Technology Letters, IEEE*, PP(99):1–1, 2014. doi:10.1109/LPT.2014.2369827.
- [4] H. Soda, K.-i. Iga, C. Kitahara, and Y. Suematsu, "GaInAsP/InP surface emitting injection lasers," *Japanese Journal of Applied Physics*, 18(12):2329, 1979.
- [5] K. Iga, "Vertical-Cavity Surface-Emitting Laser: Its Conception and Evolution," *Japanese Journal of Applied Physics*, 47(1R):1, 2008.
- [6] K. Takahashi, A. Yoshikawa, and A. Sandhu. *Wide bandgap semiconductors: fundamental properties and modern photonic and electronic devices*. Springer, 2007.
- [7] H. Amano, M. Kito, K. Hiramatsu, and I. Akasaki, "P-type conduction in Mg-doped GaN treated with low-energy electron beam irradiation (LEEBI)," *Japanese Journal of Applied Physics*, 28(12A):L2112, 1989.
- [8] S. Nakamura, T. Mukai, and M. Senoh, "High-power GaN pn junction blue-light-emitting diodes," *Japanese Journal of Applied Physics*, 30(12A):L1998, 1991.
- [9] T. Yokogawa, S. Yoshii, A. Tsujimura, Y. Sasai, and J. Merz, "Electrically pumped CdZnSe/ZnSe blue-green vertical-cavity surface-emitting lasers," *Japanese journal of applied physics*, 34(6B):L751, 1995.
- [10] A. A. Bergh, "Blue laser diode (LD) and light emitting diode (LED) applications," *physica status solidi (a)*, 201(12):2740–2754, 2004. doi:10.1002/pssa.200405124.

## REFERENCES

---

- [11] D. Feezell, “The evolving GaN VCSEL,” *Compound Semiconductor*, 20(1):44–49, 2014.
- [12] J. Hecht, “Photonic Frontiers: Nitride VCSELs: Nitride VCSELs pose a tough challenge,” *Laser Focus World*, 50:34–36, 2014.
- [13] R. Shimada and H. Morkoc, “Wide Bandgap Semiconductor-Based Surface-Emitting Lasers: Recent Progress in GaN-Based Vertical Cavity Surface-Emitting Lasers and GaN-/ZnO-Based Polariton Lasers,” *Proceedings of the IEEE*, 98(7):1220–1233, 2010.
- [14] M. Panjehpour, C. E. Julius, M. N. Phan, T. Vo-Dinh, and S. Overholt, “Laser-induced fluorescence spectroscopy for in vivo diagnosis of non-melanoma skin cancers,” *Lasers in surgery and medicine*, 31(5):367–373, 2002.
- [15] T. Vo-Dinh, M. Panjehpour, B. F. Overholt, C. Farris, F. P. Buckley, and R. Sneed, “In vivo cancer diagnosis of the esophagus using differential normalized fluorescence (DNF) indices,” *Lasers in surgery and medicine*, 16(1):41–47, 1995.
- [16] R. Stevenson, “Solid-State Lighting: Are Laser Diodes The Logical Successors To LEDs?,” *Compound Semiconductor*, 19(8):40–44, 2013.
- [17] J. Y. Tsao, M. H. Crawford, M. E. Coltrin, A. J. Fischer, D. D. Koleske, G. S. Subramania, G. Wang, J. J. Wierer, and R. F. Karlicek, “Toward Smart and Ultra-efficient Solid-State Lighting,” *Advanced Optical Materials*, 2(9):809–836, 2014.
- [18] “Blue LED inventors speak about their work ahead of Nobel awards ceremony,” *The Japan Times*, 2014.
- [19] H. Morkoç. *Handbook of Nitride Semiconductors and Devices, Materials Properties, Physics and Growth*, volume 1. John Wiley & Sons, 2009.
- [20] T. Lei, M. Fanciulli, R. Molnar, T. Moustakas, R. Graham, and J. Scanlon, “Epitaxial growth of zinc blende and wurtzitic gallium nitride thin films on (001) silicon,” *Applied physics letters*, 59(8):944–946, 1991.
- [21] M. Paisley, Z. Sitar, J. Posthill, and R. Davis, “Growth of cubic phase gallium nitride by modified molecular-beam epitaxy,” *Journal of Vacuum Science & Technology A*, 7(3):701–705, 1989.
- [22] M. Mizuta, S. Fujieda, Y. Matsumoto, and T. Kawamura, “Low temperature growth of GaN and AlN on GaAs utilizing metalorganics and hydrazine,” *Japanese journal of applied physics*, 25(12A):L945, 1986.
- [23] M. Stutzmann, O. Ambacher, M. Eickhoff, U. Karrer, A. Lima Pimenta, R. Neuberger, J. Schalwig, R. Dimitrov, P. Schuck, and R. Grober, “Playing with polarity,” *physica status solidi (b)*, 228(2):505–512, 2001.

- 
- [24] O. Ambacher, J. Smart, J. Shealy, N. Weimann, K. Chu, M. Murphy, W. Schaff, L. Eastman, R. Dimitrov, L. Wittmer, et al., “Two-dimensional electron gases induced by spontaneous and piezoelectric polarization charges in N- and Ga-face AlGaIn/GaN heterostructures,” *Journal of Applied Physics*, 85(6):3222–3233, 1999.
- [25] G. Rossbach. *High-Density Excitonic Effects in GaN*. PhD thesis, EPFL, 2014.
- [26] G. Rossbach, M. Rössischer, P. Schley, G. Gobsch, C. Werner, C. Cobet, N. Esser, A. Dadgar, M. Wieneke, A. Krost, et al., “Valence-band splitting and optical anisotropy of AlN,” *physica status solidi (b)*, 247(7):1679–1682, 2010.
- [27] R. Goldhahn, C. Buchheim, P. Schley, A. T. Winzer, and H. Wenzel, “Optical constants of bulk nitrides,” *Nitride Semiconductor Devices: Principles and Simulation*, page 95, 2007.
- [28] J. Piprek, R. Farrell, S. DenBaars, and S. Nakamura, “Effects of built-in polarization on InGaIn-GaN vertical-cavity surface-emitting lasers,” *Photonics Technology Letters, IEEE*, 18(1):7–9, 2006.
- [29] U. Strauß, A. Avramescu, T. Lerner, D. Queren, A. Gomez-Iglesias, C. Eichler, J. Müller, G. Brüderl, and S. Lutgen, “Pros and cons of green InGaIn laser on c-plane GaN,” *physica status solidi (b)*, 248(3):652–657, 2011.
- [30] D. Sizov, R. Bhat, and C.-E. Zah, “Gallium indium nitride-based green lasers,” *Journal of Lightwave Technology*, 30(5):679–699, 2012.
- [31] F. Della Sala, A. Di Carlo, P. Lugli, F. Bernardini, V. Fiorentini, R. Scholz, and J.-M. Jancu, “Free-carrier screening of polarization fields in wurtzite GaN/InGaIn laser structures,” *Applied physics letters*, 74(14):2002–2004, 1999.
- [32] G. Zhang, Y. Tong, Z. Yang, S. Jin, J. Li, and Z. Gan, “Relationship of background carrier concentration and defects in GaN grown by metalorganic vapor phase epitaxy,” *Applied physics letters*, 71(23):3376–3378, 1997.
- [33] J. Jayapalan, B. Skromme, R. Vaudo, and V. Phanse, “Optical spectroscopy of Si-related donor and acceptor levels in Si-doped GaN grown by hydride vapor phase epitaxy,” *Applied physics letters*, 73(9):1188–1190, 1998.
- [34] W. Götz, N. Johnson, J. Walker, D. Bour, and R. Street, “Activation of acceptors in Mg-doped GaN grown by metalorganic chemical vapor deposition,” *Applied Physics Letters*, 68(5):667–669, 1996.
- [35] S. Nakamura, M. Senoh, S.-i. Nagahama, N. Iwasa, T. Yamada, T. Matsushita, Y. Sugimoto, and H. Kiyoku, “Room-temperature continuous-wave operation of InGaIn multi-quantum-well structure laser diodes,” *Applied Physics Letters*, 69(26):4056–4058, 1996.

- [36] M. Kneissl and J. RaSS, "Laser diodes in the visible spectral range: GaN-based blue and green laser diodes," In H. Weber, P. Loosen, and R. Poprawe, editors, *Laser Systems*, volume 3 of *Landolt-Börnstein - Group VIII Advanced Materials and Technologies*, pages 22–37. Springer Berlin Heidelberg, 2011. doi:10.1007/978-3-642-14177-5\_3.
- [37] S.-C. Wang, T.-C. Lu, C.-C. Kao, J.-T. Chu, G.-S. Huang, H.-C. Kuo, S.-W. Chen, T.-T. Kao, J.-R. Chen, and L.-F. Lin, "Optically pumped GaN-based vertical cavity surface emitting lasers: technology and characteristics," *Japanese Journal of Applied Physics*, 46(8S):5397, 2007.
- [38] E. Felton, G. Christmann, J. Dorsaz, A. Castiglia, J.-F. Carlin, R. Butté, N. Grandjean, S. Christopoulos, G. B. H. von Högersthal, A. Grundy, et al., "Blue lasing at room temperature in an optically pumped lattice-matched AlInN/GaN VCSEL structure," *Electronics Letters*, 43(17):924–926, 2007.
- [39] P. Mackowiak and W. Nakwaski, "Some aspects of designing an efficient nitride VCSEL resonator," *Journal of Physics D: Applied Physics*, 34(6):954, 2001.
- [40] P. Mackowiak, R. P. Sarzala, M. Wasiak, and W. Nakwaski, "Design guidelines for fundamental-mode-operated cascade nitride VCSELs," *Photonics Technology Letters, IEEE*, 15(4):495–497, 2003.
- [41] T.-C. Lu, C.-C. Kao, H.-C. Kuo, G.-S. Huang, and S.-C. Wang, "CW lasing of current injection blue GaN-based vertical cavity surface emitting laser," *Applied Physics Letters*, 92(14):–, 2008. doi:http://dx.doi.org/10.1063/1.2908034.
- [42] Y. Higuchi, K. Omae, H. Matsumura, and T. Mukai, "Room-temperature CW lasing of a GaN-based vertical-cavity surface-emitting laser by current injection," *Applied Physics Express*, 1(12):121102, 2008.
- [43] T.-C. Lu, S.-W. Chen, T.-T. Wu, P.-M. Tu, C.-K. Chen, C.-H. Chen, Z.-Y. Li, H.-C. Kuo, and S.-C. Wang, "Continuous wave operation of current injected GaN vertical cavity surface emitting lasers at room temperature," *Applied Physics Letters*, 97(7):–, 2010. doi:http://dx.doi.org/10.1063/1.3483133.
- [44] K. Omae, Y. Higuchi, K. Nakagawa, H. Matsumura, and T. Mukai, "Improvement in lasing characteristics of GaN-based vertical-cavity surface-emitting lasers fabricated using a GaN substrate," *Applied Physics Express*, 2(5):052101, 2009.
- [45] D. Kasahara, D. Morita, T. Kosugi, K. Nakagawa, J. Kawamata, Y. Higuchi, H. Matsumura, and T. Mukai, "Demonstration of blue and green GaN-based vertical-cavity surface-emitting lasers by current injection at room temperature," *Applied Physics Express*, 4(7):072103, 2011.
- [46] T. Onishi, O. Imafuji, K. Nagamatsu, M. Kawaguchi, K. Yamanaka, and S. Takigawa, "Continuous wave operation of GaN vertical cavity surface emitting lasers at room temperature," *IEEE Journal of Quantum Electronics*, 48(9):1107–1112, 2012.

- [47] C. Holder, J. S. Speck, S. P. DenBaars, S. Nakamura, and D. Feezell, "Demonstration of Nonpolar GaN-Based Vertical-Cavity Surface-Emitting Lasers," *Applied Physics Express*, 5(9):092104, 2012.
- [48] G. Cosendey, A. Castiglia, G. Rossbach, J.-F. Carlin, and N. Grandjean, "Blue monolithic AlInN-based vertical cavity surface emitting laser diode on free-standing GaN substrate," *Applied Physics Letters*, 101(15):-, 2012. doi:<http://dx.doi.org/10.1063/1.4757873>.
- [49] W.-J. Liu, X.-L. Hu, L. Y. Ying, J.-Y. Zhang, and B.-P. Zhang, "Room temperature continuous wave lasing of electrically injected GaN-based vertical cavity surface emitting lasers," *Applied Physics Letters*, 104(25):-, 2014. doi:<http://dx.doi.org/10.1063/1.4885384>.
- [50] T.-C. Lu, J.-R. Chen, S.-W. Chen, H.-C. Kuo, C.-C. Kuo, C.-C. Lee, and S.-C. Wang, "Development of GaN-based Vertical-cavity Surface-emitting Lasers," *Selected Topics in Quantum Electronics, IEEE Journal of*, 15(3):850–860, 2009.
- [51] G. Cosendey, J.-F. Carlin, N. A. Kaufmann, R. Butté, and N. Grandjean, "Strain compensation in AlInN/GaN multilayers on GaN substrates: Application to the realization of defect-free Bragg reflectors," *Applied Physics Letters*, 98(18):181111, 2011.
- [52] T. Ive, O. Brandt, H. Kostial, T. Hesjedal, M. Ramsteiner, and K. H. Ploog, "Crack-free and conductive Si-doped AlN/GaN distributed Bragg reflectors grown on 6H-SiC(0001)," *Applied Physics Letters*, 85(11):1970–1972, 2004. doi:<http://dx.doi.org/10.1063/1.1791738>.
- [53] J. Piprek, "What is the problem with GaN-based VCSELs?," In *Numerical Simulation of Optoelectronic Devices (NUSOD), 2013 13th International Conference on*, pages 89–90. IEEE, 2013.
- [54] Evatec Process Systems, "LEDs & OLEDs," Online: <http://www.evatecnet.com/markets/optoelectronics/leds/leds-and-oleds-brochure>, 2012. Last checked: 2014-12-28.
- [55] S. S. Thöny, H. Friedli, M. Padrun, A. Castiglia, G. Cosendey, and N. Grandjean, "Damage-free ITO deposition on LED devices," In *IWN2012 - International Workshop on Nitride Semiconductors - Abstract Book*, pages ThP–OD–20, 2012.
- [56] M. Stattin, C. J. Lockhart de la Rosa, J. Sun, A. Yurgens, and Å. Haglund, "Metal-free graphene as transparent electrode for GaN-based light-emitters," *Japanese Journal of Applied Physics*, 52, 2013.
- [57] T. Minami, "Transparent conducting oxide semiconductors for transparent electrodes," *Semiconductor Science and Technology*, 20(4):S35, 2005. doi:[10.1088/0268-1242/20/4/004](https://doi.org/10.1088/0268-1242/20/4/004).

## REFERENCES

---

- [58] J. Sheu, Y.-K. Su, G.-C. Chi, P. Koh, M. Jou, C. Chang, C. Liu, and W. Hung, "High-transparency Ni/Au ohmic contact to p-type GaN," *Applied Physics Letters*, 74(16):2340–2342, 1999.
- [59] S. Nakamura, "The Roles of Structural Imperfections in InGaN-based Blue Light-Emitting Diodes and Laser Diodes," *Science*, 281(5379):956–961, 1998. doi:10.1126/science.281.5379.956.
- [60] D. T. S. Watson-Parris. *Carrier localization in InGaN/GaN quantum wells*. PhD thesis, University of Manchester, 2011.
- [61] B.-S. Cheng, Y.-L. Wu, T.-C. Lu, C.-H. Chiu, C.-H. Chen, P.-M. Tu, H.-C. Kuo, S.-C. Wang, and C.-Y. Chang, "High Q microcavity light emitting diodes with buried AlN current apertures," *Applied Physics Letters*, 99(4):041101, 2011.
- [62] M. Ohya, K. Fukuda, I. Masumoto, S. Kohmoto, K. Naniwae, M. Yamada, M. Matsudate, T. Tsukuda, T. Akagawa, and C. Sasaoka, "High-power operation of inner-stripe GaN-based blue-violet laser diodes," volume 6485, pages 648505–648505–9, 2007.
- [63] W.-S. Tan, K. Takahashi, V. Bousquet, A. Ariyoshi, Y. Tsuda, M. Ohta, and M. Kauer, "Blue-violet inner stripe laser diodes using lattice matched AlInN as current confinement layer for high power operation," *Applied Physics Express*, 2(11):112101, 2009.
- [64] A. Castiglia, D. Simeonov, H. Buehlmann, J.-F. Carlin, E. Feltin, J. Dorsaz, R. Butté, and N. Grandjean, "Efficient current injection scheme for nitride vertical cavity surface emitting lasers," *Applied Physics Letters*, 90(3):033514–033514, 2007.
- [65] J. S. Gustavsson, J. A. Vukusic, J. Bengtsson, and A. Larsson, "A comprehensive model for the modal dynamics of vertical-cavity surface-emitting lasers," *IEEE Journal of Quantum Electronics*, 38(2):203–212, 2002.
- [66] J. Bengtsson, J. Gustavsson, A. Larsson, A. Bachmann, K. Kashani-Shirazi, M.-C. Amann, et al., "Diffraction loss in long-wavelength buried tunnel junction VCSELs analyzed with a hybrid coupled-cavity transfer-matrix model," *Optics Express*, 16(25):20789–20802, 2008.
- [67] C. J. Chang-Hasnain and W. Yang, "High-contrast gratings for integrated optoelectronics," *Advances in Optics and Photonics*, 4(3):379–440, 2012.
- [68] M. C. Huang, Y. Zhou, and C. J. Chang-Hasnain, "A surface-emitting laser incorporating a high-index-contrast subwavelength grating," *Nature Photonics*, 1(2):119–122, 2007.
- [69] P. Gilet, N. Olivier, P. Grosse, K. Gilbert, A. Chelnokov, I.-S. Chung, and J. Mørk, "High-index-contrast subwavelength grating VCSEL," volume 7615, pages 76150J–76150J–8, 2010. doi:10.1117/12.840884.

- 
- [70] C. Chase, Y. Rao, W. Hofmann, and C. J. Chang-Hasnain, "1550 nm high contrast grating VCSEL," *Optics express*, 18(15):15461–15466, 2010.
- [71] T. Ansbæk, I.-S. Chung, E. S. Semenova, and K. Yvind, "1060-nm tunable Monolithic High Index Contrast Subwavelength Grating VCSEL," *Photonics Technology Letters, IEEE*, 25(4):365–367, 2013.
- [72] W. Hofmann, C. Chase, M. Muller, Y. Rao, C. Grasse, G. Böhm, M.-C. Amann, and C. J. Chang-Hasnain, "Long-wavelength high-contrast grating vertical-cavity surface-emitting laser," *Photonics Journal, IEEE*, 2(3):415–422, 2010.
- [73] C. Sciancalepore, B. B. Bakir, S. Menezo, X. Letartre, D. Bordel, and P. Viktorovitch, "III-V-on-Si Photonic Crystal Vertical-Cavity Surface-Emitting Laser Arrays for Wavelength Division Multiplexing," *Photonics Technology Letters, IEEE*, 25(12):1111–1113, 2013.
- [74] J. Kim, D.-U. Kim, J. Lee, H. Jeon, Y. Park, and Y.-S. Choi, "AlGaN membrane grating reflector," *Applied Physics Letters*, 95(2):021102, 2009.
- [75] T. T. Wu, Y. C. Syu, S. H. Wu, W. T. Chen, T. C. Lu, S. C. Wang, H. P. Chiang, and D. P. Tsai, "Sub-wavelength GaN-based membrane high contrast grating reflectors," *Optics Express*, 20(18):20551–20557, 2012.
- [76] Y. Wang, T. Wu, T. Tanae, H. Zhu, and K. Hane, "The resonant III-nitride grating reflector," *Journal of Micromechanics and Microengineering*, 21(10):105025, 2011.
- [77] Y. Wang, Z. Shi, X. Li, S. He, M. Zhang, and H. Zhu, "Surface-normal emission from subwavelength GaN membrane grating," *Optics Express*, 22(1):667–672, 2014.
- [78] J. Lee, S. Ahn, H. Chang, J. Kim, Y. Park, and H. Jeon, "Polarization-dependent GaN surface grating reflector for short wavelength applications," *Optics express*, 17(25):22535–22542, 2009.
- [79] T.-T. Wu, S.-H. Wu, T.-C. Lu, and S.-C. Wang, "GaN-based high contrast grating surface-emitting lasers," *Applied Physics Letters*, 102(8):081111, 2013.
- [80] M. Rommel, B. Nilsson, P. Jedrasik, V. Bonanni, A. Dmitriev, and J. Weis, "Sub-10nm resolution after lift-off using HSQ/PMMA double layer resist," *Microelectronic Engineering*, 110:123–125, 2013.
- [81] S. Krishnamoorthy, F. Akyol, P. S. Park, and S. Rajan, "Low resistance GaN/InGaN/GaN tunnel junctions," *Applied Physics Letters*, 102(11):–, 2013. doi:<http://dx.doi.org/10.1063/1.4796041>.
- [82] S. Krishnamoorthy, T. F. Kent, J. Yang, P. S. Park, R. C. Myers, and S. Rajan, "Gdn nanoisland-based gan tunnel junctions," *Nano Letters*, 13(6):2570–2575, 2013. PMID: 23662669. doi:[10.1021/nl4006723](https://doi.org/10.1021/nl4006723).

## REFERENCES

---

- [83] M. Malinverni, D. Martin, L. Lugani, L. Lahourcade, and N. Grandjean, "Buried tunnel junction for micro-LEDs and VCSELs," In *Proc. of SPIE*. International Society for Optics and Photonics, 2015.
- [84] D. Adolph and T. Ive, "Nucleation and epitaxial growth of ZnO on GaN (0001)," *Applied Surface Science*, 307:438–443, 2014.
- [85] S. Pearton, W. Lim, F. Ren, and D. Norton, "Wet Chemical Etching of Wide Bandgap Semiconductors-GaN, ZnO and SiC," *ECS Transactions*, 6(2):501–512, 2007.
- [86] C. O. Holder, J. T. Leonard, R. M. Farrell, D. A. Cohen, B. Yonkee, J. S. Speck, S. P. DenBaars, S. Nakamura, and D. F. Feezell, "Nonpolar III-nitride vertical-cavity surface emitting lasers with a polarization ratio of 100 percent fabricated using photoelectrochemical etching," *Applied Physics Letters*, 105(3):-, 2014. doi:<http://dx.doi.org/10.1063/1.4890864>.